A Linearized Model for Lithium Ion Batteries and Maps for their Performance and Failure

Rajlakshmi Purkayastha
Materials Department,
University of California,
Santa Barbara, CA 93106

Robert M. McMeeking
Materials Department and
Department of Mechanical Engineering,
University of California,
Santa Barbara, CA 93106;
School of Engineering
Aberdeen University, King's College
Aberdeen AB24 3UE, Scotland;
INM - Leibniz Institute for New Materials,
D-66123 Saarbrücken, Germany

A linearized model is developed for lithium ion batteries, relying on simplified characterizations of lithium transport in the electrolyte and through the interface between the electrolyte and the storage particles of the electrodes. The model is valid as a good approximation to the behavior of the battery when it operates near equilibrium, and can be used for both discharge and charging of the battery. The rate of extraction of lithium from and to the electrode storage particles can be estimated from the results of the model, information that can be used in turn to estimate the shrinkage and swelling stresses that develop in the particles. Given specified rates of extraction for spherical particles, maps of the resulting shrinkage and swelling stresses can be developed connecting their values to battery parameters such as particles size, diffusion coefficient, lithium partial molar volume, and particle elastic properties. Since a constant rate of extraction can only be achieved for a limited period of time until the concentration of lithium at the particle perimeter constrains the lithium mass transport, plots of the average state of charge in the particle versus time are also produced. [DOI: 10.1115/1.4005962]

Introduction

A schematic of a Li-ion battery is shown in Fig. 1. In typical current designs, the anode consists of graphite or some other form of carbon, in particulate form, embedded in a polymeric binder, with contact among the carbonaceous particles ensuring electrical conductivity. The aggregate is connected to a copper current collector [1]. The cathode has a hierarchical structure with a particulate aggregate of a compound oxide of lithium embedded in a PVDF binder [2]. These particles are joined together by electronically conducting elements to provide current connectivity, usually in the form of carbon coatings on the storage particles. The cathode aggregate is attached to an aluminum current collector. Electrical leads are connected to the two collectors and attach to the load during discharge, and to the power supply during charging. The electrolyte is a lithium salt such as $LiPF_6$ in an organic solvent, and the separator is a porous polymer, an example being a polyolefin [1].

During discharge, as depicted in Fig. 1, Li^+ ions are extracted from the graphite and travel from the anode to the cathode through the electrolyte, diffusing through the pores of the separator [1]. In parallel, electrons are released from the anode and then flow round the electrical load circuit to the cathode collector. The electrons thereafter transfer to the oxide particles. Upon reaching the cathode, the Li^+ ions are inserted into the particles of layered oxide, while the newly arrived electrons engage in an electrochemical reaction that reduces the lithium.

The charging cycle is simply the opposite of the discharge phase [1]. When a power supply is attached to the cell to charge it, the Li^+ ions travel from the positive electrode to the negative one, as shown in Fig. 1. In this process the lithium ions are oxidized and extracted from the storage particles in the positive electrode and reduced at the negative electrode by the arriving electrons and intercalated into the graphite. Thus the lithium ions simply shuttle back and forth from one electrode to the other and back during the full service cycle [2]. Note that during charging the electrode on the left is functioning as the cathode and that on the right as the anode. While it is conventional to refer to the electrode on the left in Fig. 1 always as the anode and to that on the right always as the cathode, the fact that their functions interchange depending on whether charging or discharge is occurring can cause confusion. As a result, the electrode on the left in Fig. 1 is often referred to as the negative electrode and that on the right as the positive one, as this identification is correct both during discharge and charging.

A major source of damage arises because the storage particles shrink and swell as the Li^+ ions are extracted and inserted. Depending on which particle is used, as much as 100% of the lithium is depleted from the oxide during charging [2], leading to significant shrinkage. For example, in $LiMn_2O_4$, depletion of lithium to 20% of stoichiometry leads to a volume reduction of 6.5% [3]. Upon very fast charging, the first batch of lithium extracted from the oxide particle will deplete from near its surface, causing a high tensile hoop stress as the outer layer shrinks. The resulting stress can cause cracks to propagate and damage the material. Thus, comminution of oxide particles can occur during charging

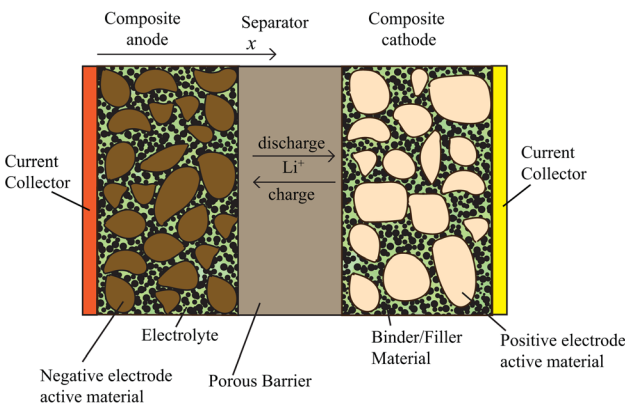

Fig. 1 Schematic of a Li-ion battery showing the main components, namely the current collectors, the electrodes, anode and cathode, and the separator. The electrodes are composed of active storage particles, binder, and filler, with electrolyte filling the pores within the particulate structure.

Contributed by the Applied Mechanics Division of ASME for publication in the JOURNAL OF APPLIED MECHANICS. Manuscript received September 4, 2011; final manuscript received November 18, 2011; accepted manuscript posted February 13, 2012; published online April 4, 2012. Assoc. Editor: Huajian Gao.

[4], a damage mechanism that can also accumulate by fatigue upon repeated cycling of the battery. Similar effects are possible in the carbonaceous material in the anode, where 8% swelling by volume occurs in graphite when the number of lithium atoms per C ring is increased from 0 to 0.6 [3]. Such damage is observed in electrode material, and is associated with a degradation of performance [5–7]. Although new materials are being proposed for lithium storage electrodes that have reduced swelling and shrinkage [8], so that the generation of tensile cracking would be obviated, other materials with large storage capacity and much greater swelling, of the order of 300%, are under development [1,7,9]. Clearly such materials are associated with very significant stress and strain generation during transient charge and discharge processes [10].

The strains associated with swelling and shrinkage of lithium storage materials can have disruptive effects on the electrode aggregate [4]. The storage and binding particles and the conducting elements can be degraded by fatigue or excessive stress as the particles swell and shrink. Furthermore, deformation of the binder caused by swelling and shrinkage of the storage particles may cause the conducting particles embedded in the binder to fail to percolate, thereby disrupting the electronic conducting path, and increasing the internal resistance of the cell. Similarly, interface layers formed on the particles can be disrupted by cracking and can spall off due to the strains of the storage particles as lithium is extracted and inserted [3,4,7]. As well as leading to secondary fracture of the storage particles and their comminution, such cracking of the surface layers demands their recreation on the exposed storage material surface, a side reaction that will consume lithium [4,7]. Such processes deplete the capacity of the cell because the total energy at full charge is proportional to the number of Li^+ ions that can be stored in the anode. Comminution of storage particles can cause much greater depletion of lithium in the cell, as large amounts of new surface will be created and then coated with an interface layer when a particle is split. This aspect of Li-ion battery performance is the main reason why the use of very small storage particles is precluded, despite the fact that they would limit the problems of fatigue crack growth, particle fracture, and comminution. Too much Li would be sequestered as a consequence of surface layer growth on very small particles, leading to a severe penalty on the capacity of the battery.

Other mechanisms of degradation of the electrodes can occur where stress and deformation do not play a role [4,11–16]. Side reactions with the electrolyte can dissolve electrode particles and reprecipitate new phases and interface layers, resulting in further sequestration of lithium, but with the added effect that the rate of diffusion of Li^+ through the resulting thicker layers slows, thereby prolonging charging times and diminishing maximum power [4,11]. At high rates of charging and discharging, structural disordering and phase changes in the electrode storage materials may occur [4,11], resulting in slowing of the rate at which lithium can be inserted and extracted, and also diminishing the capacity of the cell. Most of these ageing mechanisms are associated with reactions with the electrolyte and its organic solvent that cause their decomposition, and the production of volatile and combustible gases, along with the generation of pressure that may rupture the cell container [2,4]. In addition, there can be effects indirectly related to the electrochemistry of the cell, such as corrosion of components of the electrodes, including the current collector, oxidation of conductive particles within the electrode and its binder, and binder decomposition, especially at high charging voltages [2,4]. It has also been observed that swelling of the electrodes and external loads on the battery pack can cause creep straining of the separator, leading to closure of its pores [17]. This can lead to performance degradation as transport of Li through the separator is impeded.

Following the early work of Doyle et al. [18], there has been an intensive effort to model and simulate the performance of Li-ion batteries and the stresses generated in their storage particles. An overview of the contributions of Newman and associates, along with research from other sources, is available by Thomas et al. [19]. Commonly, mixture theories and a mean field approach, referred to as porous electrode theory, are used to represent the complex microstructure of the electrodes and separator, analyzed in a one-dimensional (1D) approximation through the thickness of the battery foil [3,7,18–26]. The results are used to study insertion and extraction of Li to and from storage particles, leading to stress generation, the effect of strain and contact stress on electrical conductivity, and the transients and accumulation of damage in cells. Garcia et al. [27,28] utilized a two-dimensional (2D) simulation of porous electrode microstructures, identifying elements of the battery architecture such as storage particles, binder, and electrolyte pores for specific realizations of the microstructure. Beyond this, Sastry and co-workers [29–31] have utilized random particle networks to analyze Li mass transport and electronic conductivity in electrodes as they swell and shrink, including the effects of phase transformation, and have used the outcomes to assess the stress in particles of various shapes. Based on these 1D, 2D, and 3D methodologies, the conditions experienced by the active particles in the electrodes can be predicted as they swell and shrink due to insertion and extraction of lithium, and ageing [19,21,23], including interface film growth [32], and thermal runaway [33–37] have been treated. Multiscale methods have also been used to study the performance of Li-ion batteries, such as the work of Golman et al. [38] on electrochemical-mechanical interactions in cells. In addition, Bohn et al. [39] have based their study of mass transport and stress generation in storage particles on models of the Li chemical potential encompassing excess Gibbs free energy, and therefore are able to simulate the effect of phase change and staging in the storage particles.

Fracture of particles has been a major focus of research based on the analysis of intercalation and stress generation in single particles, such as that of Verbrugge and Koch [40]. For example, Aifantis and Dempsey [41] have modeled crack growth in storage particles, as have Cheng and Verbrugge [42]. Criteria for avoiding fracture have been developed by Cheng and Verbrugge [43], while Zhao et al. [44] consider the effect of fast charging on the generation of fracture in particles. Further studies of fracture in storage particles have been provided by Yang [45], Woodford et al. [46], the latter based on concepts of thermal shock, and by Bhandakkar and Gao [47,48], who use cohesive zone models to predict fracture of electrodes and their minimum size to ensure a comminution proof system. Studies of the implications of very large intercalation strains associated with such storage materials as silicon [9,10] with regard to modeling of the associated mechanics, stress generation, inelastic deformation, and interactions at the electrochemical-mechanical level have also been carried out [49,50].

A glance at any one of the papers referenced above will convince the reader of the complexity of the formulations considered necessary to adequately model a Li-ion battery. In view of this challenge to modeling and simulation, work has been carried out to simplify and reduce the order of the partial differential and algebraic equations involved. An early effort in this regard was that of Botte and White [51] who considered whether diffusion driven by stress gradients in storage particles could be ignored, though their conclusion is that such effects are significant and stress effects on mass transport cannot be neglected. Other approaches have included model reformulations for Li-ion batteries to improve parameter estimation, optimal design, and numerical computation efficiency [52], while Renganathan and White [53] consider semianalytical approximations and integration methods to ease the burden of computation. Similarly, Ramadesigan et al. [54] reformulate the governing equations of solid-state diffusion to enhance computational efficiencies, Forman et al. [55] have introduced quasi-linearization of the porous electrode equations and a Padé approximation for the solution for the diffusion of Li in spherical particles, and Gallagher et al. [56] have simplified the model for interface impedance between the electrolyte and storage particles in the porous electrode. We note

that in this regard that some further possibilities have not been explored, namely aggressive linearization and full simplification of the mass transport and electrochemical kinetics involved in Li-ion batteries. The objective of this paper is to present such an approach and to provide the solutions that can thereby be obtained. These solutions are valid in specific limits, such as when the battery operates close to equilibrium and has sluggish, negatively charge ions in the electrolyte. Furthermore, the solutions, being exact, can serve as benchmarks for computational methods designed to solve the fully nonlinear, coupled equations for battery performance. In addition, we develop particle stress and charge/discharge maps for batteries based on equally simplified assumptions, with the advantage that these maps are relatively easy to generate and can thus be made comprehensive without much effort.

Elementary Linearized Model

We assume porous electrode theory with homogeneous properties for the battery in regard to the spatial coordinates other than x, where x is defined according to Fig. 1. Therefore we consider governing equations only in regard to the independent variables x and time t, and seek planar solutions describing the behavior of an infinitely extended battery in directions orthogonal to x. We note that many batteries are configured in the form of a foil that has been rolled up, and we assume that the radius of curvature of the roll is not so small as to compromise the planar behavior we analyze. We make no attempt to describe the full set of equations that govern porous electrode theory for Li-ion batteries, given their complexity [18], but instead simply state the linearized, simplified formulation. The resulting equations can then be compared with the full nonlinear formulation both for Li-ion batteries [18] and for electrochemistry and mass transport of ionic species in general [57].

Each electrode is characterized by its volume fraction f_i of storage particles, which will determine the capacity of the battery. Note that $i=n$ for the negative electrode and $i=p$ for the positive one. In addition, the volume fractions of binder, electronically conducting coatings, and pore space for electrolyte are relevant, but we do not define them as we will not introduce models for how these parameters influence electronic conductivity, ionic impedance, Li mass transport, etc. Instead, we will simply work with the relevant, average macroscopic quantities, such as the average electrode electronic resistivity ρ_i and the average electrode ionic resistivity R_i. We note that electronic conductivity is associated with paths through the conducting coatings applied to storage particles, and through graphite particles if present, whereas ionic conductivity is associated with paths through the electrolyte. Mass transport of Li within the storage particles is not considered to be a contributor to the ionic conductivity of the electrode. Note that the separator has average ionic resistivity R_s but is considered to have zero electronic conductivity. As with the electrodes, we make no attempt to connect the separator porosity to its average ionic resistivity. Finally, we assume that the current collectors are perfect electronic conductors but are impermeable to Li^+ and other ions.

There are two assumptions that are critical to our ability to linearize and simplify the governing equations. The first of these assumptions is that we take the negative ions in the electrolyte to be immobile, so that the ionic current in the electrolyte is entirely due to the Li^+ ions. This assumption seems acceptable because typically the negative ion in the Li-ion battery electrolyte is a large anion such as PF_6^- [1], and therefore likely to be much less mobile than Li^+. Furthermore, for lack of data on ionic mobility in multicomponent electrochemical mass transport, the complex governing equations are often simplified through arbitrary assumption, so that our inference of zero mobility for the anion in the electrolyte is consistent with common, pragmatic usage. As a consequence of this assumption, the concentration of the salt (e.g., $LiPF_6$) remains uniform during mass transport of the Li^+ ion to ensure charge neutrality. Therefore, gradients of concentration of the salt are absent, and the only driving force for transport of the Li^+ is the electric field in the electrolyte. Hence transport of Li^+ is controlled by the kinetic relationship

$$E = iR_i \tag{1}$$

where $E=E(x,t)$ is the electric field in the electrolyte and $i=i(x,t)$ is the current density. Note that we define the current density to be the current per unit cross-sectional area of the battery, and not per unit area of electrolyte pores. Therefore the actual current density in the electrolyte is i divided by the electrolyte pore volume fraction. In addition, and for obvious reasons, the ionic resistivity R_i of the electrode is calibrated consistent with the definition of current density, and is divided by the battery area (not the pore area) and multiplied by the electrode thickness to obtain the total electrode resistance. In view of our 1D model, the electric field E acts in the x direction and the current density i conveys charge in the x direction. Note that i is positive when Li^+ is traveling in the positive x direction (see Fig. 1), and the flux J^e_{Li} of Li^+ in the electrolyte is given by

$$J^e_{Li} = \frac{i}{F} \tag{2}$$

where F is Faraday's constant in Coulombs per mole. The flux J^e_{Li} is defined in terms of moles per unit time per unit battery area and not per unit electrolyte pore area. We note that Eqs. (1) and (2) apply to the separator as well as to the electrodes. In the separator $i=I$, where I is the total current density for the battery, as it is a current loop. As with all quantities, the current density I is defined per unit area of the battery. In contrast, in the electrodes the electronic current density in the phases conducting electrons is $I-i$.

The Li^+ ions are being extracted from and inserted into the storage particles. Let $Q=Q(x,t)$ be the resulting source term defined as the flux of Li^+ entering the electrolyte per unit volume of the electrode per unit time. As a consequence,

$$\frac{\partial J^e_{Li}}{\partial x} = Q \tag{3}$$

We note that we are neglecting the flux of charge that is involved in setting up the charge double layer on the surface of the electrode particles [57]. Such charge double layers are inherent to the electrochemistry of electrodes and when accounted for give the electrode surface a capacitance and a characteristic time for the creation and relaxation of the double layer. However, we assume that the time scale involved in modifying the charge double layer is not rate limiting and so neglect its influence in our governing equations.

In general, the flux of Li^+ ions to and from the storage particles is governed by Butler-Volmer kinetics [57] in the form

$$j = \frac{i_o}{F}\left[\exp\left(\frac{\alpha_a F}{RT}\eta_s\right) - \exp\left(-\frac{\alpha_c F}{RT}\eta_s\right)\right] \tag{4}$$

where j is the flux of Li^+ ions leaving the storage particles (in moles per unit time per unit area of particle surface), $i_o = i_o(c, c_s, T)$ is the exchange current density, a function of the concentration c of Li^+ in the electrolyte, the concentration c_s of Li in the storage particle at its surface, and of the temperature T. The parameters α_a and α_c are transfer coefficients, $\eta_s = \Phi_s - \Phi_e - U(c, c_s, T)$ is known as the surface overpotential, where Φ_s is the potential of the particle surface, Φ_e is the potential in the electrolyte adjacent to the particle surface, U is the open circuit potential (OCP) of the material at the particle surface, and R is the gas constant. Note that when the surface overpotential is positive, the electrode is anodic and Li is being oxidized to Li^+ and being ejected from the storage particles, with the oxidation reaction

being the signature feature that defines an anode [57]. In contrast, when the surface overpotential is negative, the electrode is cathodic and Li^+ is being reduced to Li and being inserted into the storage particles, with the reduction reaction being the signature feature that defines a cathode [57]. Note that the electrode is at equilibrium when the surface overpotential is zero and the anodic and cathodic fluxes cancel each other out.

We now come to the second crucial assumption simplifying the equations. We assume that the electrodes always operate close to equilibrium, so that the Butler-Volmer kinetics in Eq. (4) may be linearized. This leads to

$$Q = jA = \frac{i_o(\alpha_a + \alpha_c)A}{RT}\eta_s \tag{5}$$

where A is the storage particle surface area exposed to electrolyte per unit volume of the electrode. Note that the exchange current density and the transfer coefficients will be unique to the storage particle material involved. Observing that

$$E = -\frac{\partial \Phi_e}{\partial x} \tag{6}$$

we then deduce from Eqs. (1)–(3) and (5) that

$$\frac{\partial^2 \Phi_e}{\partial x^2} - \frac{R_i}{\rho_i^s}\Phi_e = \frac{R_i}{\rho_i^s}(U - \Phi_s) \tag{7}$$

where

$$\rho_i^s = \frac{RT}{i_o^i(\alpha_a^i + \alpha_c^i)A_i F} \tag{8}$$

and the subscripts and superscripts i indicate the positive or negative electrode.

Now recall that the battery is a current loop of magnitude I in terms of current density. Since i is the current density in the electrolyte path, that in the electron conducting path must be

$$i_e = I - i \tag{9}$$

Since the surfaces of the storage particles are connected to the electron conducting path, the electric field at the storage particle surface must conform to

$$-\frac{\partial \Phi_s}{\partial x} = (I - i)\rho_i \tag{10}$$

Use of Eqs. (2) and (3) and differentiation of Eq. (7) then gives us

$$\frac{\partial^3 \Phi_e}{\partial x^3} - \frac{R_i + \rho_i}{\rho_i^s}\frac{\partial \Phi_e}{\partial x} = \frac{R_i}{\rho_i^s}\left(\frac{\partial U}{\partial x} + \rho_i I\right) \tag{11}$$

as the differential equation governing each electrode. Note that we have made another important assumption—that the exchange current density is uniform throughout the active electrode, and therefore does not vary with the state of charge of the storage particles.

Positive Electrode. We now solve Eq. (11) for the potential Φ_e^p within the electrolyte in the positive electrode, where the origin is at the interface between the separator and the positive electrode, which has width w_p. This electrode therefore occupies $0 \le x \le w_p$. Boundary conditions are

$$\frac{\partial \Phi_e^p(0)}{\partial x} = -IR_p \qquad \frac{\partial \Phi_e^p(w_p)}{\partial x} = 0 \tag{12}$$

since the current at the interface with the separator is entirely ionic and at the current collector at $x = w_p$ it is entirely electronic. Therefore, within $0 \le x \le w_p$ we find

$$\Phi_e^p(x) - \Phi_e^p(0) = \frac{IR_p}{R_p + \rho_p}\left\{\sqrt{\frac{\rho_p^s}{R_p + \rho_p}}\left[\frac{(\rho_p + R_p\cosh\lambda_p w_p)(\cosh\lambda_p x - 1)}{\sinh\lambda_p w_p} - R_p\sinh\lambda_p x\right] - \rho_p x\right\} \tag{13}$$

where

$$\lambda_p = \sqrt{\frac{R_p + \rho_p}{\rho_p^s}} \tag{14}$$

and we have assumed that the OCP at the particle surface in the electrode is uniform. From Eq. (1) we then find the current density in the electrolyte path to be

$$i = \frac{I}{R_p + \rho_p}\left[\rho_p + R_p\cosh\lambda_p x - \frac{(\rho_p + R_p\cosh\lambda_p w_p)\sinh\lambda_p x}{\sinh\lambda_p w_p}\right] \tag{15}$$

and the flux of Li^+ out of particles is given by Eq. (3) as

$$Q = -\frac{I}{F\sqrt{\rho_p^s(R_p + \rho_p)}}\left[\frac{R_p\cosh\lambda_p(w_p - x) + \rho_p\cosh\lambda_p x}{\sinh\lambda_p w_p}\right] \tag{16}$$

Thereafter, from Eqs. (5) and (8) we obtain the potential Φ_s^p at the storage particle surface to be

$$\Phi_s^p(x) = \frac{I\rho_p}{R_p + \rho_p}\left\{\sqrt{\frac{\rho_p^s}{R_p + \rho_p}}\left[R_p\sinh\lambda_p x - \frac{(\rho_p + R_p\cosh\lambda_p w_p)\left(\cosh\lambda_p x + \frac{R_p}{\rho_p}\right)}{\sinh\lambda_p w_p}\right] - R_p x\right\} + \Phi_e^p(0) + U^p \tag{17}$$

where U^p is the OCP of the positive electrode with respect to a reference electrode. In particular, the potential at the current collector of the positive electrode is given by

$$\Phi_s^p(w_p) = -\frac{I}{R_p + \rho_p}\left\{\sqrt{\frac{\rho_p^s}{R_p + \rho_p}}\left[\frac{(\rho_p^2 + R_p^2)\cosh\lambda_p w_p + 2R_p\rho_p}{\sinh\lambda_p w_p}\right] + R_p\rho_p w_p\right\} + \Phi_e^p(0) + U^p \tag{18}$$

Negative Electrode. For the analysis of the negative electrode, we now place the origin at the interface between the negative electrode and the separator, with the negative electrode having width w_n. Therefore, within the electrode, in $-w_n \le x \le 0$, we find, from considerations similar to those for the positive electrode, that the potential Φ_e^n in the electrolyte is

$$\Phi_e^n(x) - \Phi_e^n(0) = \frac{IR_n}{R_n+\rho_n}\left\{\sqrt{\frac{\rho_n^s}{R_n+\rho_n}}\left[\frac{(\rho_n + R_n\cosh\lambda_n w_n)(1-\cosh\lambda_n x)}{\sinh\lambda_n w_n} - R_n\sinh\lambda_n x\right] - \rho_n x\right\}$$

$$\lambda_n = \sqrt{\frac{R_n+\rho_n}{\rho_n^s}} \tag{19}$$

while the current density in the electrolyte path is deduced to be

$$i = \frac{I}{R_n+\rho_n}\left[\frac{(\rho_n + R_n\cosh\lambda_n w_n)\sinh\lambda_n x}{\sinh\lambda_n w_n} + R_n\cosh\lambda_n x + \rho_n\right] \tag{20}$$

This leads to the flux of Li^+ out of the storage particles given by

$$Q = \frac{I}{F\sqrt{\rho_n^s(R_n+\rho_n)}}\left[\frac{R_n\cosh\lambda_n(w_n+x) + \rho_n\cosh\lambda_n x}{\sinh\lambda_n w_n}\right] \tag{21}$$

The potential Φ_s^n at the surface of the storage particles is then deduced to be

$$\Phi_s^n(x) = \frac{I\rho_n}{R_n+\rho_n}\left\{\sqrt{\frac{\rho_n^s}{R_n+\rho_n}}\left[R_n\sinh\lambda_n x + \frac{(\rho_n + R_n\cosh\lambda_n w_n)\left(\cosh\lambda_n x + \frac{R_n}{\rho_n}\right)}{\sinh\lambda_n w_n}\right] - R_n x\right\} + \Phi_e^n(0) + U^n \tag{22}$$

where U^n is the OCP of the negative electrode with respect to the same reference electrode used for the positive one. The potential at the current collector for the negative electrode is then

$$\Phi_s^n(-w_n) = \frac{I}{R_n+\rho_n}\left\{\sqrt{\frac{\rho_n^s}{R_n+\rho_n}}\left[\frac{(\rho_n^2+R_n^2)\cosh\lambda_n w_n + 2R_n\rho_n}{\sinh\lambda_n w_n}\right] + R_n\rho_n w_n\right\} + \Phi_e^n(0) + U^n \tag{23}$$

Separator. The separator carries uniform current density, so the potential difference across it is, according to our somewhat unconventional notation,

$$\Phi_e^p(0) - \Phi_e^n(0) = -IR_s w_s \tag{24}$$

Cell Potential Difference. The cell potential difference Φ is obtained by subtracting Eq. (23) from Eq. (18). The result, after use of Eq. (24), is

$$\Phi = U - \frac{I}{R_p+\rho_p}\left\{\sqrt{\frac{\rho_p^s}{R_p+\rho_p}}\left[\frac{\left(\rho_p^2+R_p^2\right)\cosh\lambda_p w_p + 2R_p\rho_p}{\sinh\lambda_p w_p}\right] + R_p\rho_p w_p\right\} - \frac{I}{R_n+\rho_n}\left\{\sqrt{\frac{\rho_n^s}{R_n+\rho_n}} \times \left[\frac{(\rho_n^2+R_n^2)\cosh\lambda_n w_n + 2R_n\rho_n}{\sinh\lambda_n w_n}\right] + R_n\rho_n w_n\right\} - IR_s w_s \tag{25}$$

where

$$U = U^p - U^n \tag{26}$$

is the OCP of the cell.

When the battery is being discharged, the current density I is positive, and the terms on the right-hand side of Eq. (25) in addition to the OCP represent the losses within the cell, and therefore everything multiplying I, when added together, gives us the internal resistance per unit area of battery. When the battery is being charged, the current density is negative, and the terms on the right-hand side of Eq. (25) in addition to U gives the additional potential in excess of the OCP that must be applied to charge the cell.

Optimal Electrode Thickness. Although a detailed study of optimization of the battery is beyond the scope of this paper, we briefly assess the implications of Eq. (25) in this regard. We note that this equation suggests that, as far as minimizing internal battery losses are concerned, there is an optimal electrode thickness; in contrast to the common view that the thinnest electrode is the best. For the purposes of the assessment, we assume that all parameters except the electrode thickness have been chosen to constitute the battery design. Such design parameters must be chosen to ensure trade-offs among competing priorities are met; e.g., a thin, low resistance separator should be chosen, but having sufficient robustness to avoid electrical breakdown, and being sufficiently stiff and strong to avoid mechanical compromises such as creep deformation; in addition, the separator must be sufficiently thick that it is impermeable to unwanted mass transport, such as diffusion of the storage materials from one electrode to the other [4]. Another example of the necessary trade-offs is that good ionic conductivity in the electrolyte of the pores of the electrode requires high pore volume, which can only be achieved by cannibalizing the space that otherwise can be allocated to storage particles. Given that all parameters other than electrode thickness have been chosen, we now ask whether there is an optimal electrode thickness for minimizing internal losses. This requires maximization of Eq. (25) with respect to w_p and w_n, a procedure that gives

$$w_p = \sqrt{\frac{\rho_p^s}{R_p+\rho_p}}\cosh^{-1}\left(1 + \frac{R_p+\rho_p}{\sqrt{R_p\rho_p}}\right) \tag{27}$$

as the optimal thickness, with an equivalent result for w_n. Clearly this result indicates that for electrode thicknesses below this level, the internal losses will rise above the optimum.

Insertion and Extraction Rate. As noted above, the flux of Li^+ into and out of particles is given by Eq. (16) in the positive electrode and Eq. (21) in the negative electrode. Note that when the current density I is positive (i.e., a battery in discharge), the positive electrode is cathodic and the flux Q being negative, indicates that Li^+ is being inserted into its storage particles; simultaneously the negative electrode is anodic and the flux Q positive, involves Li^+ being extracted from its storage particles. When the current density I is negative (a battery being charged), the situation is reversed; the positive electrode is anodic and the flux Q now positive, shows that Li^+ is extracted from its storage particles; simultaneously the negative electrode is cathodic and the flux Q now negative, indicates that Li^+ is being inserted into its storage particles. We now seek the location in the electrodes where the magnitude of the flux rate is maximized. Differentiation of Eqs. (16) and (21) with respect to x and then differentiation again shows that the magnitude of the flux may have one minimum somewhere in the middle of the electrode. Therefore, the largest flux rate is to be found on one side or the other of the electrode.

In the case of the positive electrode, when $R_p > \rho_p$ the maximum rate of Li^+ flux into or out of its storage particles occurs at the interface between the separator and the electrode. When the situation is reversed, and $R_p < \rho_p$, the maximum flux occurs at the current collector. A similar situation arises in the negative electrode. We note that the electronic conducting path is likely to be more conductive than the ionic conducting path in the electrolyte, and therefore $R_p > \rho_p$, making it more likely that the highest flux will occur in both electrodes at the interface with the separator. Based on evidence that comminution of particles is most severe at the separator [4,26], we infer that this is indeed the common situation since a high rate of extraction or insertion is more likely to lead to the high stresses that fracture particles [3,7,25–27,29–31]. We note that according to our model the flux at the interface with the separator in the positive electrode is

$$\tilde{Q}_p = -\frac{I}{F\sqrt{\rho_p^s(R_p+\rho_p)}}\left(\frac{R_p\cosh\lambda_p w_p + \rho_p}{\sinh\lambda_p w_p}\right) \tag{28}$$

and in the negative electrode it is

$$\tilde{Q}_n = \frac{I}{F\sqrt{\rho_n^s(R_n+\rho_n)}}\left(\frac{R_n\cosh\lambda_n w_n + \rho_n}{\sinh\lambda_n w_n}\right) \tag{29}$$

Battery Performance During Continuous Utilization. We now consider the performance of a charged battery if we operate it continually at constant current density I until the negative electrode is depleted of Li. We assume that the storage particles in the battery are initially at the same state of charge (SOC) having the same concentration of Li in them. At first the voltage will be given by Eq. (25) and will hold steady. We assume now that the electrodes are such that the electronic conducting paths have low resistivity compared to the ionic conducting paths. Therefore, the rate of flux for storage particles near the separator will be higher than elsewhere, and in the negative electrode these particles will be depleted of Li^+ first and in the positive electrode they will be filled first.

So far we have assumed that the exchange current density for the storage particles is constant. However, it is well known that this parameter depends on the SOC of the particles, in particular depending on the concentration of Li adjacent to the particle surface, as noted above. In addition to gradual changes to the exchange current density that occur over the normal range of SOC, an evolution that we have ignored in our model, more profound modifications take place in certain circumstances. For example, when the material near the surface is completely filled with Li to stoichiometric capacity (e.g., $x \to 1$ for Li_xCoO_2 in the case of lithium cobalt oxide) or is exhausted of Li (e.g., $x \to 0$ for Li_xCoO_2), the exchange current density changes dramatically as side reactions start to become important or new insertion phenomena begin to dominate [57]. We will model these features by simply assuming that the exchange current density goes to zero when the surface of the particle is depleted of Li or is filled. That is, extraction stops when the material near the surface of the particle is devoid of Li and insertion ceases when the material near the particle surface is stoichiometrically filled. We further simplify this picture by the assumption that Li diffusion within the particles is relatively fast, and the concentration of Li within them remains fairly uniform. As a consequence, extraction will continue in the negative electrode until the particles are completely depleted of Li and then will stop; similarly, insertion will continue in the positive electrode until the particles are filled and then will cease.

Since we have assumed that the fastest insertion and extraction rates occur in particles closest to the separator, these particles will be the first to terminate the active processes of insertion and extraction. To account for this we divide the electrodes into two regions, those adjacent to the current collectors and having thicknesses $\tilde{w}_p$ (for the positive electrode) and $\tilde{w}_n$ (for the negative electrode) that remain active, and the remainders adjacent to the separator that have become inactive for the reasons above. The regions near the separator, being passive, will simply provide ionic conducting paths in the electrolyte within them, and will no longer need to conduct electrons as none are being absorbed or released within these regions of the electrodes. As a consequence, they are annexed to the separator in terms of their function within the battery, but retaining their unique ionic resistivity. The remaining active regions of the electrodes have an unchanged function as active electrodes, but are thinner than the original electrode. As a consequence we can write the potential difference across the cell as a modification of Eq. (25) as

$$\begin{aligned}\Phi = U &- \frac{I}{R_p+\rho_p}\left\{\sqrt{\frac{\rho_p^s}{R_p+\rho_p}}\left[\frac{\left(\rho_p^2+R_p^2\right)\cosh\lambda_p\tilde{w}_p + 2R_p\rho_p}{\sinh\lambda_p\tilde{w}_p}\right] + R_p\rho_p\tilde{w}_p\right\} - \frac{I}{R_n+\rho_n}\left\{\sqrt{\frac{\rho_n^s}{R_n+\rho_n}}\right.\\ &\left.\times\left[\frac{\left(\rho_n^2+R_n^2\right)\cosh\lambda_n\tilde{w}_n + 2R_n\rho_n}{\sinh\lambda_n\tilde{w}_n}\right] + R_n\rho_n\tilde{w}_n\right\} - IR_s w_s\\ &- IR_p\left(w_p-\tilde{w}_p\right) - IR_n\left(w_n-\tilde{w}_n\right)\end{aligned} \tag{30}$$

We can regard $w_n - \tilde{w}_n$ as a measure of utilization, as it will grow once the inactive zone in the electrode has been established. We note that it is not an exact measure of utilization as the storage particles in $\tilde{w}_n$ are already partially depleted when the inactive zone is established, and, of course, there is an initial period of use of the battery during which $\tilde{w}_n = w_n$. Nevertheless, after an inactive zone is created in the electrode, $w_n - \tilde{w}_n$ can serve as a rudimentary measure of battery utilization. Furthermore, if the positive and negative electrodes have equal capacity, $\tilde{w}_p/w_p = \tilde{w}_n/w_n$, so that both $w_p - \tilde{w}_p$ and $w_n - \tilde{w}_n$ serve as equivalent measures of utilization.

Given our comments regarding the optimal electrode thickness, we deduce that the potential difference for the cell from Eq. (30) will fall beyond a certain point as $\tilde{w}_p$ and $\tilde{w}_n$ diminish. Therefore, the loss of potential typically observed in cells [18] is reproduced by the simple linearized model, in particular the significant loss that tends to accompany the end of the discharge cycle. We can make this point clearer by approximating Eq. (30) for thin electrodes so that the hyperbolic trigonometric functions can be linearized to first order. This gives

$$\begin{aligned}\Phi = U - I\left\{\frac{\rho_n^s}{\tilde{w}_n} + \frac{R_n\rho_n\tilde{w}_n}{R_n+\rho_n} + \frac{\rho_p^s}{\tilde{w}_p} + \frac{R_p\rho_p\tilde{w}_p}{R_p+\rho_p} + R_n\left(w_n-\tilde{w}_n\right)\right.\\ \left. + R_p\left(w_p-\tilde{w}_p\right) + R_s w_s\right\}\end{aligned} \tag{31}$$

making it clear that the potential difference for the cell will drop dramatically at the end of utilization. Indeed, the potential difference can even drop to zero in this process, illustrating the significant evolution the cell can experience during utilization.

We can consider reversing the process to assess charging. In this case, at the end of the charging process, as we try to completely fill Li^+ into the storage particles in the negative electrode, the voltage that must be applied to the cell to continue its charging at a given rate will rise dramatically. The alternative possibility is also interesting: if we charge the battery at a fixed voltage, the charging rate will steadily diminish at the end of the charging process.

Stress Generation in the Storage Particles. We have deduced the flux rate of Li^+ into and out of storage particles in the form of Q, the source term defined in Eqs. (3), (5), (16), and (21), with a rate at the interface with the separator given by Eqs. (28) and (29).

It is well know that the rate at which Li^+ is inserted into or extracted from storage particles determines the peak stresses in them that arise due to heterogeneous swelling and shrinkage of the particles due to the presence of Li [3,7,25–27,29–31]. Such stresses are responsible for the fracture and comminution of the storage particles. As the foregoing list of references indicates, a great deal of work has been done on this problem. However, comprehensive maps of the peak stress as a function of battery parameters have not been developed, and an objective of the present paper is to provide such maps derived from simplified, basic assumptions regarding the process of insertion and extraction of Li.

The model developed above provides us with Q, which is the flux of Li^+ per unit volume of electrode delivered by storage particles. It is desirable to connect Q to the flux rate J^s_{Li} of Li^+ leaving particles that is defined per unit surface area of storage particles. The obvious way to do that is to divide Q by the particle surface area exposed to electrolyte per unit volume of electrode, as used above in Eq. (5). However, we will calculate the diffusion of Li in spherical particles as if their entire surface area is exposed to electrolyte, so that we can take advantage of spherical symmetry to simplify the computations. Therefore the parameter we need to divide into Q is the total surface area of storage particles per unit volume of the electrode. Treating the storage particles as spheres of equal size, we find this parameter to be $3f/r_0$, where r_0 is the particle diameter. As a consequence, the equivalent flux of Li^+ ions out of spherical storage particles through their surface is

$$J^s_{Li} = \frac{Qr_0}{3f} \tag{32}$$

where we should recall that the volume fraction of storage particles in the electrode is f.

We now describe computations of mass transport of Li within spherical storage particles subject to an extraction rate J^s_{Li} at the surface such that Eq. (32) connects these computations to the macroscopic, linear battery model summarized above. Equivalently, these computations represent storage particles subject to a surface current density equal to FJ^s_{Li}, where this current is positive when directed outward from the particle surface.

Stress Maps for a Single Spherical Lithium Storage Particle

Model Description. As described earlier, the insertion and extraction of lithium into storage particles results in significant volume changes, which, over time, are thought to lead to the comminution of storage particles. While earlier studies focused solely on the electrochemistry of the battery [18,19,22,24,58,59] more recent efforts have turned toward the study of the stress generated within storage particles via coupled diffusion-stress models [3,30,31,38,39,43–49]. We utilize essentially the same methods as other workers on this topic, but we emphasize our attempt to be generic, so that we can map the generation of stress in storage particles in terms of battery performance and design parameters. In addition, we pursue a fundamentally consistent approach in terms of the model for mass transport of lithium and the mechanics of stress generation in the particles, though we confine ourselves to relatively simple versions of the system model in this paper as a first effort to lay out the general principles behind our ideas.

We start with the equation for the ideal chemical potential of lithium per mole, as determined by Bohn et al. [39], when it is intercalating a storage particle,

$$\mu_{Li} = \mu^0_{Li} + RT \ln \frac{c_{Li}}{c_{max} - c_{Li}} - \Omega_{Li}\sigma_h, \quad 0 \le c_{Li} \le c_{max} \tag{33}$$

where μ^0_{Li} is the ideal enthalpic contribution per mole of lithium when dissolved in the lattice, the second term on the right-hand side is a model for the ideal entropic contribution, and the third term is the effect due to the presence of mechanical stress. Since we use a model of the ideal chemical potential of the lithium when it is intercalated in the storage particle, we have omitted the excess Gibbs free energy term, or interaction energy, included by Bohn et al. [39] in their expression. In Eq. (33) c_{Li} is the concentration of lithium in moles per unit volume, and c_{max} is the maximum possible concentration of lithium dissolved in a storage particle, above which concentration further intercalation sites are unavailable and a new phase must form. The contribution of mechanical energy is given by $-\Omega_{Li}\sigma_h$, where Ω_{Li} is the partial molar volume of lithium dissolved in the lattice and σ_h is to the hydrostatic stress within the particle. Note that we use the simplest possible model in several respects; the intercalation solution is assumed to be ideal, the material is taken to swell or shrink isotropically when lithium is inserted or removed, the resulting strain is small and analyzed within the mechanics of infinitesimal straining, and the partial molar volume is assumed to be independent of lithium concentration.

The vector flux J_{Li} of lithium within the particle, in moles per unit area per unit time, is given by

$$J_{Li} = c_{Li} v_{Li} \tag{34}$$

where v_{Li} is the vector of average velocity of lithium, proportional to its mobility M_{Li} and the gradient of its chemical potential, so that

$$J_{Li} = -c_{Li} M_{Li} \nabla \mu_{Li} \tag{35}$$

Following [39] we take the mobility to be isotropic and a function of lithium concentration, accounting for the likelihood of a successful hop from one intercalation site to another, so that

$$M_{Li} = M_0 \left(1 - \frac{c_{Li}}{c_{max}}\right) \tag{36}$$

where the parameter M_0 is given by

$$M_0 = D_o RT \tag{37}$$

with D_o the concentration independent diffusion parameter.

On combining Eqs. (33)–(37), we find that the flux is given by

$$J_{Li} = -D_0 \left\{ \nabla c_{Li} - \left(1 - \frac{c_{Li}}{c_{max}}\right) \frac{\Omega_{Li} c_{Li}}{RT} \nabla \sigma_h \right\} \tag{38}$$

Note the important difference between this equation for lithium flux and that used by Zhang et al. [30], where the term $(1 - c_{Li}/c_{max})$ is not present. However, in the absence of a gradient of hydrostatic stress, our flux equation and that resulting from the form used by Zhang et al. [30] are the same. At least when the solution is ideal, the flux response is isotropic, the intercalation strains are small and isotropic, and the partial molar volume is independent of lithium concentration, we note that Eq. (38) is rigorous, including its accounting for the effect of a hydrostatic stress gradient, a conclusion we come to because of our rigorous formulation of the chemical potential of the lithium and its mobility. As noted by Bohn et al. [39], the term $(1 - c_{Li}/c_{max})$ in Eq. (38) brings symmetry in the effect of the hydrostatic stress gradient at both concentration extremes, $c_{Li} = 0$ and $c_{Li} = c_{max}$, where the flux arising from the hydrostatic stress gradient will be zero. This result comes about because the effects of entropy dominate the lithium chemical at these extremes of concentration, and the influence of hydrostatic stress is negligible.

Other formulations of solid-state lithium mass transport include those based on multicomponent diffusion, with the effect of stress incorporated via a pressure gradient term [3,25], a set up that is broadly consistent with our treatment above, but that leads to detail differences. In some treatments, the contribution of the

stress gradient term in lithium mass transport is neglected [40,43–45,51,60], while others go beyond ideal thermodynamics to account for interaction effects among lithium atoms as they intercalate [3,7,38,39,51]. In some cases, the relevant chemical potential is obtained from the measured OCP [3,7,39], perhaps using activity coefficients in the formulation [3,7,40,43,51].

The equation governing lithium mass transport is obtained by use of conservation of mass to obtain

$$\frac{\partial c_{\mathrm{Li}}}{\partial t} + \nabla \cdot J_{\mathrm{Li}} = 0 \tag{39a}$$

or

$$\frac{\partial c_{\mathrm{Li}}}{\partial t} = D_0 \nabla \cdot \left\{ \nabla c_{\mathrm{Li}} - \left(1 - \frac{c_{\mathrm{Li}}}{c_{\max}}\right) \frac{\Omega_{\mathrm{Li}} c_{\mathrm{Li}}}{RT} \nabla \sigma_h \right\} \tag{39b}$$

Note that we have derived our lithium transport equation in general terms, but we will use it in this paper to address only the case of a spherical particle subject to spherically symmetric, radially heterogeneous concentrations of lithium.

Swelling strains occur due to volume changes that arise during intercalation/deintercalation of lithium in the storage particle. When these strains are heterogeneous, elastic stress will also arise, so that the total strain is given by

$$\varepsilon = \frac{1}{E}[(1+\nu)\sigma - 3\nu\sigma_h I] + \frac{\Omega_{\mathrm{Li}}(c_{\mathrm{Li}} - c_0)}{3} I \tag{40}$$

where ε is the strain tensor, E is Young's modulus, ν is Poisson's ratio, I is the identity tensor, and c_0 is a datum concentration at which the swelling strain is considered to be zero. The equation for equilibrium of stress is given by

$$\nabla \cdot \sigma = 0 \tag{41}$$

Given that the free surface of the storage particle is traction free, we use the result for thermal stresses in a solid spherical body of outer radius r_0 when the temperature distribution is spherically symmetric, as derived by Timoshenko and Goodier [61] and used by Zhang et al. [30]. The radial σ_r and circumferential σ_c stresses are given by

$$\sigma_r = \frac{2\Omega_{\mathrm{Li}} E}{3(1-\nu)} \left(\frac{1}{r_0^3} \int_0^{r_0} c_{\mathrm{Li}} r^2 dr - \frac{1}{r^3} \int_0^{r} c_{\mathrm{Li}} r^2 dr \right) \tag{42}$$

$$\sigma_c = \frac{\Omega_{\mathrm{Li}} E}{3(1-\nu)} \left(\frac{2}{r_0^3} \int_0^{r_0} c_{\mathrm{Li}} r^2 dr + \frac{1}{r^3} \int_0^{r} c_{\mathrm{Li}} r^2 dr - c_{\mathrm{Li}} \right) \tag{43}$$

where r is measured from the center of the particle. The hydrostatic stress is then deduced to be

$$\sigma_h = \frac{\sigma_r + 2\sigma_c}{3} = \frac{2\Omega_{\mathrm{Li}} E}{3(1-\upsilon)} \left(\frac{1}{r_0^3} \int_0^{r_0} c_{\mathrm{Li}} r^2 dr - \frac{c_{\mathrm{Li}}}{3} \right) \tag{44}$$

From these equations one can determine that during steady extraction starting from uniform lithium concentration, the maximum principal stress is circumferential, tensile, occurs at the particle surface, and is given by

$$\sigma_{\max}(t) = \frac{\Omega_{\mathrm{Li}} E}{3(1-\nu)} \left[\frac{3}{r_0^3} \int_0^{r_0} c_{\mathrm{Li}}(r,t) r^2 dr - c_{\mathrm{Li}}(r_0,t) \right] \tag{45}$$

Boundary and Initial Conditions. Earlier work on stress in storage particles [3,30,39] was usually confined to the case of lithium insertion. In such simulations, the computation is initiated with a uniform concentration of lithium, and the insertion rate at the particle surface is uniform and constant in time, a process known as galvanostatic insertion. For obvious reasons, the lithium concentration at the surface of the particle during the insertion process is higher than elsewhere in the particle and reaches $c_{\max}$ there first. The usual procedure in these earlier simulations is to stop the computation at this stage. An alternative to the simulations just described is to couple the computation of stress in the particle to a battery simulator such as Dualfoil [3,7,18–20] that predicts the insertion rate for particles in the electrode as a function of time and position through the thickness of the electrode. Such a procedure allows the continuation of the computation beyond the steady insertion rate stage of the process as the coupling between the battery simulator and the individual particle allows for the evolution of the boundary conditions at the particle surface through the use of Butler-Volmer kinetics. For example, in the actual charging of a battery, after a predetermined average lithium concentration in the negative electrode is reached, the battery is held at a constant potential for a while in order to equalize the concentration among and within the storage particles. The coupling of the particle stress computation with the battery simulator enables this transition to be allowed for.

More recently, simulations of lithium extraction from particles have been undertaken and the resulting stress in them predicted. These have been carried out in both fashions just described; i.e., on the one hand, lithium is removed from the particle surface at a constant and uniform rate (i.e., galvanostatic extraction), with the simulation terminated when the lithium concentration at the particle surface reaches a minimum level [46,62]; on the other hand, the extraction simulation can be carried out with the particle stress computation coupled to a battery simulator [25,26].

To avoid the limitations of simulations of purely galvanostatic extraction, but to obviate the need to couple the storage particle stress computation to a battery simulator, we mimic conditions experienced by spherical storage particles during actual battery charging and discharge by doing the following.

In the case of extraction, the particle has a uniform initial lithium concentration $c_{\mathrm{Li}} = c_{\max}$. The particle is discharged galvanostatically, with uniform lithium flux through its entire free surface, until the surface reaches the minimum permitted lithium concentration, i.e., until $c_{\mathrm{Li}}(r_0,t) = 0$. Thereafter, the concentration at the particle surface is held fixed at $c_{\mathrm{Li}}(r_0,t) = 0$ while the extraction process continues. The simulation can be continued for an arbitrary time, but for practical reasons we terminate insertion when the average value of $c_{\mathrm{Li}}/c_{\max}$ within the particle becomes equal to 0.01. Note that the average value of $c_{\mathrm{Li}}/c_{\max}$ in the negative electrode is known as the state of charge (SOC). We will adopt this terminology for individual storage particles indiscriminately, using the term SOC as defined above for any storage particle, notwithstanding whether it is for the positive or negative electrode.

Note that the procedure just described is a reasonable approximation to what is experienced by a storage particle during battery charging or discharge. At first the process is close to being galvanostatic, because the surface overpotential and exchange current density do not vary greatly as lithium is extracted. Then, when the lithium concentration at the particle surface reaches its extreme (i.e., $c_{\mathrm{Li}}(r_0,t) = 0$), the surface overpotential and exchange current density adjust in such a way that the lithium concentration at the particle surface remains close to its extreme value (i.e., close to $c_{\mathrm{Li}}(r_0,t) = 0$), a result that comes about because of the tendency for side reactions to become dominant and because the Gibbs free energy of the new phases that develop beyond these extremes is relatively high.

Furthermore, the surface concentration of lithium in the storage particle determines the lithium chemical potential there (at least in the absence of stress at the free surface, see Eq. (33)). Note that the OCP of the particle surface is directly related to the lithium chemical potential by

$$FU^s(t) = \tilde{\mu}_{\mathrm{Li}} - \mu_{\mathrm{Li}}(r_0,t) \tag{46}$$

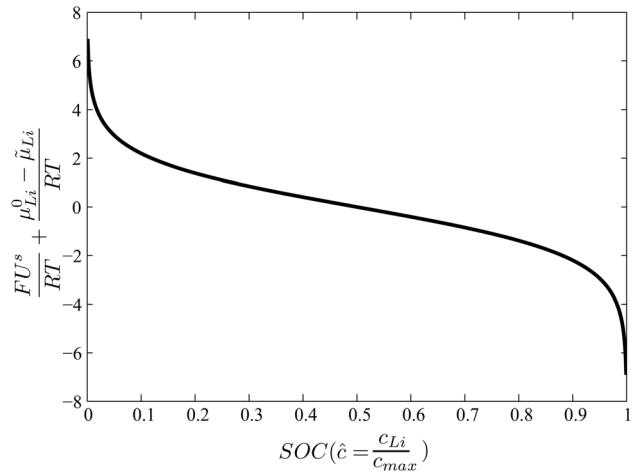

Fig. 2 Plot of the open circuit potential (OCP) versus the state of charge (SOC) for an electrode having ideal thermodynamics

where $\tilde{\mu}_{\mathrm{Li}}$ is the lithium chemical potential in the reference electrode used to define the OCP for the electrode within which the given storage particle lies. (Note that for reference purposes we have plotted in Fig. 2 the OCP from Eq. (46), subject to Eq. (33), as a function of the SOC for a particle having a uniform lithium concentration, and therefore zero stress. For a battery designed to have the same lithium capacity in both electrodes the variation of the battery OCP would be twice what is shown in Fig. 2, so that this figure is representative of the OCP for a battery having ideal electrodes in which the lithium chemical potential for both electrodes is represented by expressions having the form of Eq. (33).)

It follows that when the particle surface is held at a fixed potential and the electrolyte potential adjacent to it does not vary, such a condition is tantamount to holding the lithium concentration at the particle surface fixed. For this reason, a boundary condition on the mass transport process for lithium in which the lithium concentration at the storage particle surface is held fixed is known as a potentiostatic process. Thus the stage of battery charging during which the potential difference between the electrodes is held constant while the surface lithium concentration in the particles has reached its extreme value (i.e., $c_{\mathrm{Li}}(r_0,t) = 0$) is a potentiostatic process. The same can be said for battery discharge if the control system for battery utilization holds the potential difference between the electrodes fixed. In summary, we are therefore modeling the effects on a storage particle during battery charging and discharge as a galvanostatic process taking the surface lithium concentration from one extreme value to another (i.e., from $c_{\mathrm{Li}}(r_0,t) = c_{\max}$ to $c_{\mathrm{Li}}(r_0,t) = 0$) followed by a potentiostatic process in which the surface lithium concentration is held fixed (i.e., at $c_{\mathrm{Li}}(r_0,t) = 0$).

During the galvanostatic stage of our simulations, the flux of lithium out of a storage particle through its surface is given by Eq. (32). As is standard practice in the literature, this boundary condition will be stated in terms of a surface current density i_n defined as current exiting the particle when positive, such that

$$J_r(r_0,t) = J^s_{\mathrm{Li}} = \frac{Qr_0}{3f} = \frac{i_n}{F} \tag{47}$$

where J_r is the radial component of the vector J_{Li}.

Nondimensionalization. In order to ensure that the study is generic and applicable to a wide range of materials, battery designs, and performance indicators, the equations are nondimensionalized. Following Zhang et al. [30] we use the nondimensionalized position, time, Li concentration, and surface current density given by

$$\hat{r} = \frac{r}{r_0} \quad \hat{t} = \frac{tD_0}{r_0^2} \quad \hat{c}_{\mathrm{Li}} = \frac{c_{\mathrm{Li}}}{c_{\max}} \quad \hat{I} = \frac{i_n r_0}{FD_0 c_{\max}} \tag{48}$$

Although it would be more natural to nondimensionalize the stress tensor by dividing it by $\Omega_{\mathrm{Li}} c_{\max} E$ since this group sets the scale for the stress components [43,62], we prefer to normalize the stress tensor by Young's modulus alone as we believe the resulting values are more informative and, of course, the result represents the scale of the elastic strains. In addition, we introduce a new parameter as the nondimensionalized partial molar volume so that

$$\hat{\sigma} = \frac{\sigma}{E} \quad \hat{\Omega} = \frac{\Omega_{\mathrm{Li}} E}{RT} \tag{49}$$

Note that there is an additional nondimensional parameter, namely Poisson's ratio ν, and another elucidated below.

In nondimensional form, the diffusion equation for lithium transport in the storage particle reduces to

$$\frac{\partial \hat{c}_{\mathrm{Li}}}{\partial \hat{t}} = \left(\frac{\partial}{\partial \hat{r}} + \frac{2}{\hat{r}}\right)\left[\frac{\partial \hat{c}_{\mathrm{Li}}}{\partial \hat{r}} - \hat{\Omega}(1 - \hat{c}_{\mathrm{Li}})\hat{c}_{\mathrm{Li}} \frac{\partial \hat{\sigma}_h}{\partial \hat{r}}\right] \tag{50}$$

During the galvanostatic stage of extraction, the boundary condition is

$$\frac{\partial \hat{c}_{\mathrm{Li}}(1,\hat{t})}{\partial \hat{r}} = -\hat{I} + \hat{\Omega}[1 - \hat{c}_{\mathrm{Li}}(1,\hat{t})]\hat{c}_{\mathrm{Li}}(1,\hat{t}) \frac{\partial \hat{\sigma}_h(1,\hat{t})}{\partial \hat{r}} \tag{51}$$

whereas in the potentiostatic stage the boundary condition is

$$\hat{c}_{\mathrm{Li}}(1,\hat{t}) = 0 \tag{52}$$

The formulas for stress, Eqs. (43) and (44), can be stated in nondimensional form. We give only the result for hydrostatic stress,

$$\hat{\sigma}_h = \frac{2\varepsilon^{\max}_{\mathrm{Li}}}{3(1-\nu)}\left(\int_0^1 \hat{c}_{\mathrm{Li}} \hat{r}^2 d\hat{r} - \frac{\hat{c}_{\mathrm{Li}}}{3}\right) \tag{53}$$

where

$$\varepsilon^{\max}_{\mathrm{Li}} = \Omega_{\mathrm{Li}} c_{\max} \tag{54}$$

is the final dimensionless parameter, representing the maximum swelling strain that can be induced by the lithium.

We observe that the relevant solutions for the dimensionless lithium concentration and the dimensionless stress tensor as functions of dimensionless position in the storage particle and dimensionless time will depend only on the three irreducible parameters, $\hat{I}$, $\hat{\Omega}$, and $\varepsilon^{\max}_{\mathrm{Li}}$. Therefore, all solutions can be phrased in terms of these three parameters and we now proceed to explore the territory of particle stresses and SOC in that context. We note that Zhang et al. [30] published a plot for the maximum principal stress during lithium galvanostatic insertion as a function of $\hat{I}$ for spherical $Li_xMn_2O_4$ particles, with the modulus taken to be 10 GPa. While their stress results can be normalized by their modulus to give results in dimensionless form, they pertain to only one specific value of $\hat{\Omega}$ and one specific value of $\varepsilon^{\max}_{\mathrm{Li}}$. Thus we will augment their results by considering solutions for an appropriate range of values of $\hat{I}$, $\hat{\Omega}$, and $\varepsilon^{\max}_{\mathrm{Li}}$, although we will confine ourselves to extraction in this paper.

For guidance on the appropriate range for the parameters, we consider storage particles composed of lithium manganate ($Li_xMn_2O_4$) and use parameters taken from literature [3,30,46]:

$$D_0 = 7.08 \times 10^{-15}\ \mathrm{m}^2/\mathrm{s}$$

$$\Omega_{\mathrm{Li}} = 3.497 \times 10^{-6}\ \mathrm{m}^3/\mathrm{mol}$$

$$E = 100\ \mathrm{GPa}$$

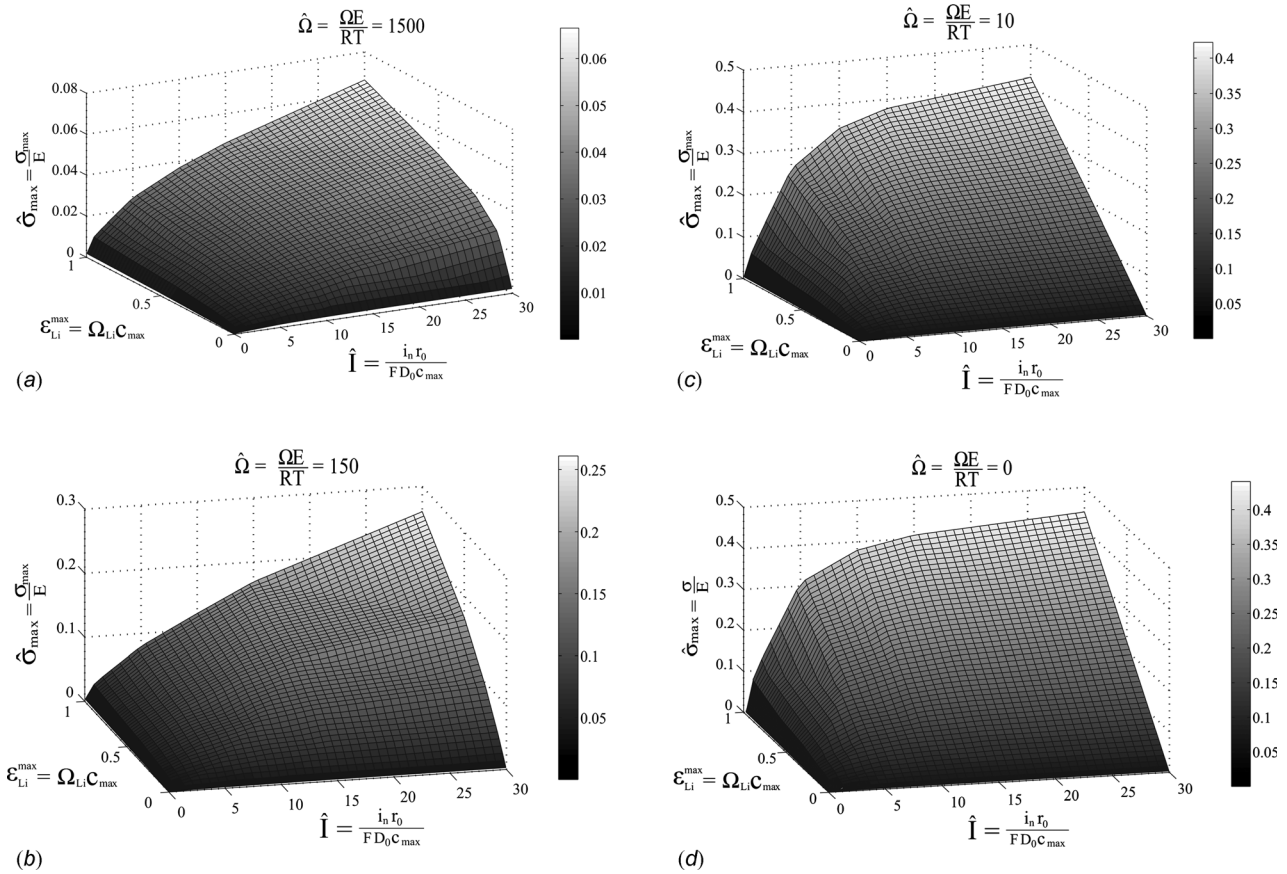

Fig. 3 Three-dimensional stress maps generated for (*a*) $\hat{\Omega} = 1500$, (*b*) $\hat{\Omega} = 150$, and (*c*) $\hat{\Omega} = 10$, where $\hat{\Omega}$ is the normalized lithium partial molar volume. The peak maximum principal stress during galvanostatic extraction followed by potentiostatic extraction is shown as a function of the normalized lithiation strain ε_{Li}^{max} and the normalized extraction rate $\hat{I}$.

Thus $\hat{\Omega} = 141$ for $Li_xMn_2O_4$.

For a spherical particle of radius 15 μm at a surface current density of 31.3 A/m^2 the nondimensional current is 30. Such a rate insertion corresponds to discharge at 10 C, i.e., the entire particle will be filled in 1/10th of an hour or 6 min. This would be a relatively high rate of insertion or extraction for a particle, and can therefore be considered to be an upper limit.

A typical maximum upper limit for the lithium concentration in lithium manganate storage particles is $c_{max} = 2.29 \times 10^4$ mol/m^3. As a consequence, the value for ε_{Li}^{max} for lithium manganate is 0.08.

Taking these numbers as a baseline, we choose a range of values extending from 0 to 1500 for $\hat{\Omega}$, from 0.5 to 30 for $\hat{I}$, and from 0.005 to 1.0 for ε_{Li}^{max}. Of course, a strain of unity for lithiation is somewhat beyond the limit where infinitesimal strain theory is truly valid, but we include such a high lithiation strain because new storage materials such as silicon tend to swell a great deal when they absorb lithium. In addition, the elastic strains produced when ε_{Li}^{max} is high are actually more modest, so that the use of infinitesimal theory is just about acceptable. We should note, however, that there are other issues, such as the distinction between undeformed and deformed configuration and its effect on the equations of mass transport that become of concern when the lithiation swelling is large, but we have ignored such complications.

A note should be made concerning the value of $\hat{\Omega} = 0$. This does not imply that either the Young's modulus or the partial molar volume is zero. At extremely high temperatures, i.e., $T \to \infty$, $\hat{\Omega} \to 0$. This is consistent with the fact that at high temperatures entropy driven diffusion will dominate, and the contribution of the stress gradient term will be negligible or zero. This observation justifies the inclusion of results for $\hat{\Omega} = 0$ for completeness, though, of course, we realize that very high temperatures are physically unrealistic in the operation of batteries.

Results. For the case of extraction, the circumferential stress at the surface is the maximum tensile stress experienced in the particle. In Fig. 3 we provide plots of such maximum stresses experienced in the particle during extraction as a function of the dimensionless current $\hat{I}$ and the maximum lithiation strain ε_{Li}^{max} at various values of $\hat{\Omega}$. As one would expect, increasing the values of $\hat{I}$ and ε_{Li}^{max} leads to an increase in the maximum stress experiences by the particle. The monotonically increasing dependence of the maximum stress on the maximum lithiation strain occurs for obvious reasons, as the latter is the parameter that controls all strain magnitudes, including elastic ones, in the extraction or insertion process. As noted by others [30], the fact that the extraction rate $\hat{I}$ determines the gradient of lithium concentration in the particles leads to the monotonic dependence of the maximum stress in the particle on the extraction rate. That is, a large gradient in the concentration of lithium, leading to large gradients of lithiation strain, requires a large elastic strain in compensation and thus produces a large maximum stress.

We note that the elastic strains predicted in Fig. 3 are relatively high, up to 5% in one case and 40% in another. This partly reflects the fact that the maximum lithiation strains can be relatively high; e.g., 8% in the case of lithium manganate as noted above. It seems likely that the elastic strain levels observed at the higher end in Fig. 3, and the associated stresses, are likely to fracture and comminute storage particles. However, the extraction rates and the lithiation strains in practice will enable avoidance of the extreme

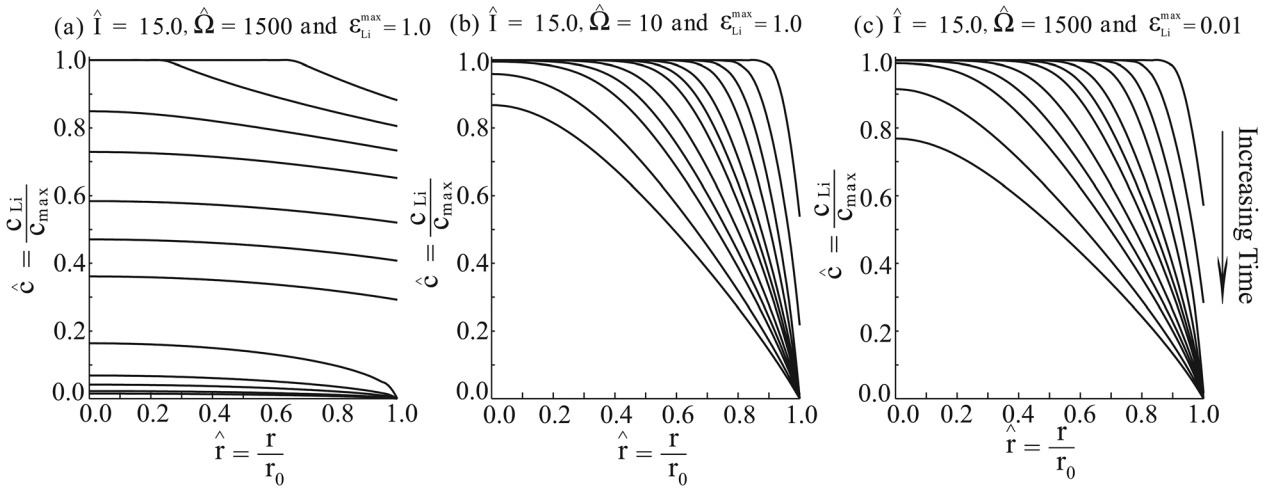

Fig. 4 Lithium concentration profile in a storage particle at specific times for particular values of the normalized extraction rate $\hat{I}$, the normalized lithium partial molar volume $\hat{\Omega}$, and the normalized lithiation strain ε_{Li}^{max}: (*a*) $\hat{I} = 15$, $\hat{\Omega} = 1500$, $\varepsilon_{Li}^{max} = 1.0$; (*b*) $\hat{I} = 15$, $\hat{\Omega} = 10$, $\varepsilon_{Li}^{max} = 1.0$; and (*c*) $\hat{I} = 15$, $\hat{\Omega} = 1500$, $\varepsilon_{Li}^{max} = 0.01$

strain magnitudes possible in the conditions encompassed by Fig. 3. For example, as we have already discussed, the lithium manganate in a battery charging at 10 C with particles of diameter 30 μm has $\hat{I} = 30$, $\hat{\Omega} = 141$, and $\varepsilon_{Li}^{max} = 8\%$. Such a condition leads to a dimensionless maximum stress approaching 30%. While such a discharge rate is relatively rapid, the example illustrates that the elastic strains and associated stresses in storage particles can in practice be quite high, suggesting that they are actually quite robust and resistant to fracture and comminution. Nevertheless, it seems likely that even at lower extraction rates comparable to 1 C that are common in practice, fracture, and comminution of storage particles is always a real possibility.

We note that the maximum stress during extraction, according to Fig. 3, is highest when $\hat{\Omega}$ is low and lower when $\hat{\Omega}$ is high. This inverse dependence on $\hat{\Omega}$ is at first sight surprising, as $\hat{\Omega}$ is proportional to the partial molar volume of lithium intercalating the storage particle, and thus one might expect stresses to go up as $\hat{\Omega}$ increases. The observed dependence of the maximum principal stress on $\hat{\Omega}$ arises because of the role it plays in the lithium transport equation, Eq. (50). A high value of $\hat{\Omega}$ enhances the influence of stress gradients on lithium flux, whereas a low $\hat{\Omega}$ value limits the influence of stress gradients. We note that the stress gradient in the storage particle will always aide the process that is being undertaken; i.e., during extraction the hydrostatic stress at the particle surface is positive, whereas at its center the hydrostatic stress is negative. Thus, in the case of extraction the hydrostatic stress gradient set up by the extraction process will speed the rate at which the lithium is transported. As a consequence, the gradients of lithium concentration in the storage particle during extraction will be less severe when $\hat{\Omega}$ is large and more severe when it is small.

Since the lithium concentration is the cause of the swelling that leads to the elastic stresses, we can conclude that the magnitudes of stress will be relatively small when $\hat{\Omega}$ is large. This phenomenon is confirmed by the results in Fig. 4 which shows the profile of lithium concentration in the storage particle at various stages of the extraction process, commencing with the particle full of lithium. The plot in Fig. 4(*a*) is for a case at the extreme of the spectrum we have studied, having a high value of each of the dimensionless parameters that control the behavior, with $\hat{\Omega} = 1500$ to be specific, so that the influence of the hydrostatic stress gradient on lithium transport is very strong. It can be seen that the lithium concentration remains fairly uniform throughout the particle during the extraction process, with only a slight gradient from the particle surface to its center. Only at the end of galvanostatic extraction, when the concentration at the particle perimeter approaches and reaches zero, is there a significant gradient in the lithium concentration. Recall that the elastic stresses, and thus the maximum principal stress, are highest when the lithium concentration gradient is greatest; it follows that the stress in this case will remain everywhere relatively small, with a peak in its magnitude only toward the end of galvanostatic extraction and at the beginning of the potentiostatic stage. This is confirmed by the results in Fig. 5(*a*) which shows the maximum principal stress in the storage particle for this case, among others, as a function of time. It can be seen that the maximum principal stress rises to a peak at the end of galvanostatic extraction and falls thereafter. The probable reason why the maximum principal stress is greatest at the end of galvanostatic extraction is that $\hat{c}_{Li}$ approaches and reaches zero at that time, and thus the influence of the hydrostatic stress gradient at the particle surface is de-emphasized and almost eliminated (see Eq. (50)). Thus the lithium flux near the surface slows down and a greater gradient of the lithium concentration is required to keep the transport process going. This in turn leads to an enhancement of the maximum principal stress, leading to the trend observed in Fig. 5(*a*) for the case under consideration. After the process has switched over to potentiostatic extraction, the lithium gradient naturally declines as time passes, and as a consequence the maximum principal stress also diminishes with time.

Now consider the case illustrated by the results in Fig. 4(*b*), which is the same as that for Fig. 4(*a*) except that the value of $\hat{\Omega}$ is much smaller, at 10. It can be seen that the profile of the lithium concentration in the particle is very different in this case, as compared to the results in Fig. 4(*a*). As time passes throughout galvanostatic extraction, the lithium concentration near the center of the particle is almost unchanged from its initial value. Only near the particle surface is the lithium concentration reduced by the extraction process, and as a consequence there is a steep gradient there. This leads to the much higher maximum principal stress that is found in this case, as illustrated by the results in Fig. 3(*c*). In contrast to the result given in Fig. 4(*a*), the contribution to the lithium flux due to the hydrostatic stress gradient in the case illustrated in Fig. 4(*b*) is relatively low, requiring steeper gradients in the lithium concentration gradient to ensure consistency of the lithium flux with the boundary condition, namely $\hat{I} = 15$. As a consequence, the stress generated in the particle is greater than for the case used to generate Fig. 4(*a*). This confirms our reasoning as to why a high $\hat{\Omega}$ leads to a low maximum principal stress in the particle and vice versa. We note also that the distribution of lithium in the case illustrated in Fig. 4(*b*) will lead to the highest maximum principal stress at the end of galvanostatic extraction, a fact that is confirmed by the relevant result in Fig. 5(*c*) where the

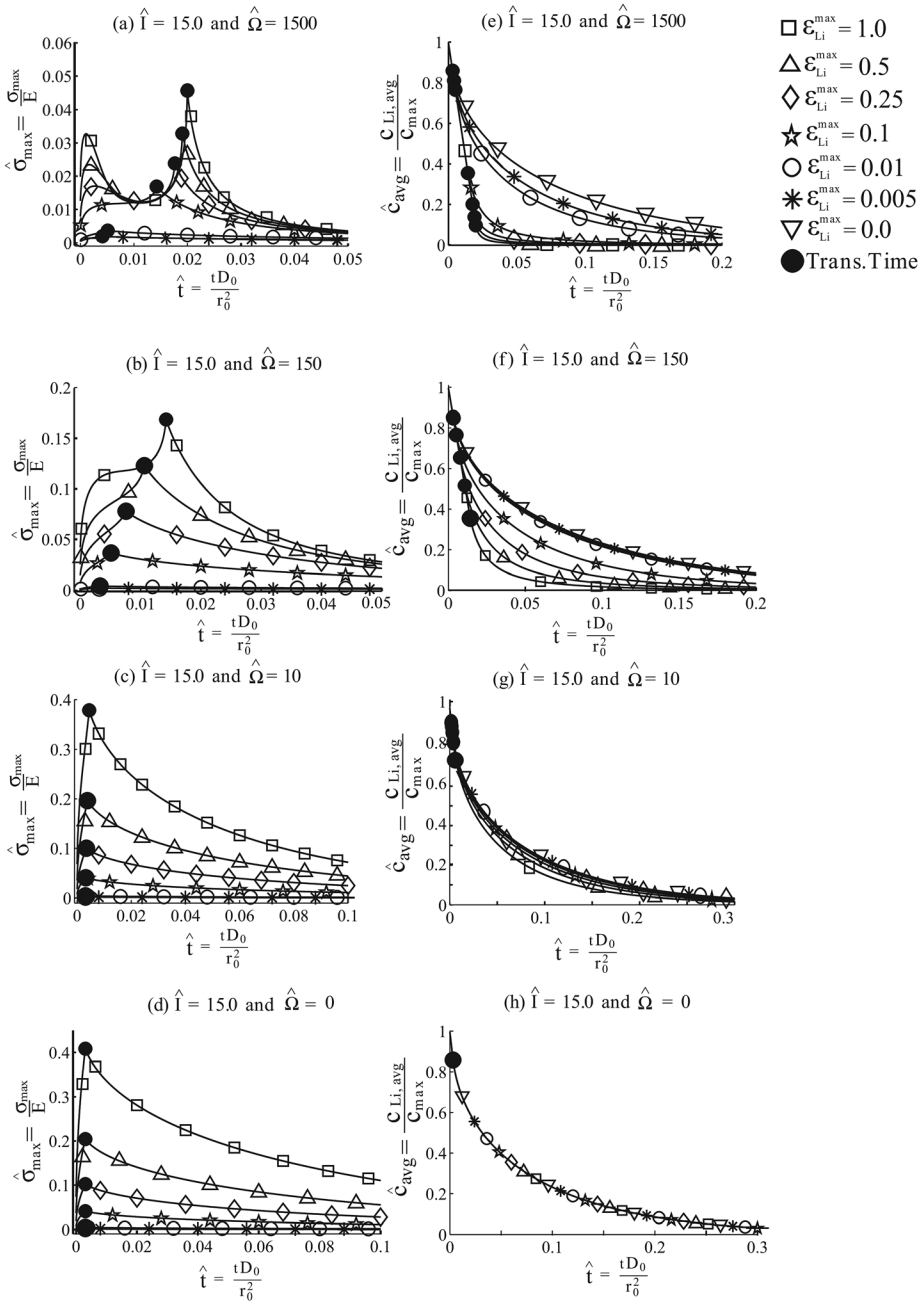

Fig. 5 Histories of maximum principal stress (*a*)–(*d*) and average lithium concentration (SOC) (*e*)–(*h*) in a storage particle during galvanostatic extraction followed by potentiostatic extraction. The normalized extraction rate is $\hat{I} = 15$ and results are shown for four values of the normalized lithium partial molar volume $\hat{\Omega}$. Within each plot results for different values of the normalized lithiation strain ε_{Li}^{max} are provided. (*a*) Maximum principal stress for $\hat{\Omega} = 1500$; (*b*) maximum principal stress for $\hat{\Omega} = 150$; (*c*) maximum principal stress for $\hat{\Omega} = 10$; (*d*) maximum principal stress for $\hat{\Omega} = 0$; (*e*) SOC for $\hat{\Omega} = 1500$; (*f*) SOC for $\hat{\Omega} = 150$; (*g*) SOC for $\hat{\Omega} = 10$; and (*h*) SOC for $\hat{\Omega} = 0$.

stress peaks at that stage, and at a much higher value than the equivalent result in Fig. 5(*a*).

Note also that Fig. 4(*c*) illustrates that reducing the maximum lithiation strain ε_{Li}^{max} while keeping $\hat{\Omega}$ constant has a similar effect on the lithium concentration gradient as keeping ε_{Li}^{max} constant and reducing $\hat{\Omega}$. The reasons for this effect are very similar to those associated with the effect of $\hat{\Omega}$ on the lithium concentration gradient. At a given gradient of lithium concentration, a high value of ε_{Li}^{max} leads to high stress magnitudes, whereas a low value causes low stress magnitudes. Because the average stress in the particle must be zero, an effect that is due to the absence of tractions on the particle surface, high stress magnitudes lead to high stress gradients, i.e., during extraction a high tension at the particle surface and a high compression at its center. The high stress gradient enhances the lithium flux and so the particle is evacuated of lithium much more rapidly. To maintain a given extraction rate, it follows that a particle having a high value of ε_{Li}^{max} will experience lower gradients of lithium concentration, while a particle having a low value of ε_{Li}^{max} will experience higher gradients of lithium concentration. This feature is confirmed by the contrasting results in Figs. 4(*a*) and 4(*c*). However, the increased gradients of lithium concentration in the case depicted in Fig. 4(*c*) are associated with

lower magnitudes of maximum principal stress despite the tendency for high gradients of lithium concentration to promote high maximum principal stresses, a consequence of the low value of $\varepsilon_{\mathrm{Li}}^{\max}$ and thus the low magnitudes of elastic strain that are generated.

We now explore the results in Fig. 5 more thoroughly. In this figure the SOC for a storage particle is shown as a function of time as well as the maximum principal stress in it, as mentioned above. Results are shown for a high extraction rate $\hat{I} = 15$ and for various values of $\hat{\Omega}$ and $\varepsilon_{\mathrm{Li}}^{\max}$. The time at which the transition from galvanostatic to potentiostatic extraction occurs is marked in each case by a black dot. The results in Figs. 5(*a*)–5(*d*) indicate for the cases considered that the peak maximum principal stress during extraction occurs at the transition from galvanostatic to potentiostatic extraction. The maximum principal stress thereafter falls because potentiostatic extraction involves a process in which the lithium concentration gradients tend to diminish in time, and thus stress levels go down. It might be expected that high stress levels would be achieved shortly after extraction commences because of large lithium concentration gradients that would be expected near the particle surface. The results in Fig. 5 show that such high stresses near the beginning of extraction are most notable in the case of $\hat{\Omega} = 1500$, but are otherwise not very significant. Even in the case of $\hat{\Omega} = 1500$, after peaking, these early time stress levels fall and only rise again later to higher levels as galvanostatic extraction is coming to an end. It is likely that the high stresses in the case of $\hat{\Omega} = 1500$ that occur shortly after the beginning of extraction occur because the hydrostatic stress gradient term in the lithium transport equation (Eq. (50)) is less significant at the beginning when $\hat{c}_{\mathrm{Li}}$ is close to unity because of the presence of the factor $1 - \hat{c}_{\mathrm{Li}}$. This feature will make early stage extraction when $\hat{\Omega} = 1500$ similar to other cases in that the high driving force for hydrostatic stress gradient driven lithium flux that otherwise prevails when $\hat{\Omega} = 1500$ is de-emphasized. Thus, high lithium concentration gradients associated with high stress gradients can build up in the early stages of extraction, but are then dissipated as $\hat{c}_{\mathrm{Li}}$ falls significantly below unity due to the fact that the hydrostatic stress gradient driven flux becomes more significant. In contrast, the process of the high stresses building up in time continues unabated in the cases for which $\hat{\Omega} \neq 1500$ and this build up only terminates when galvanostatic extraction is brought to an end.

The results in Figs. 5(*e*)–5(*h*) show the storage particle SOC as a function of time for various values of the dimensionless parameters $\hat{\Omega}$ and $\varepsilon_{\mathrm{Li}}^{\max}$ for an extraction rate of $\hat{I} = 15$. The transition from galvanostatic to potentiostatic extraction is shown by a black dot, so that the relative duration of these two stages is illustrated. Obviously the SOC is linear with time during galvanostatic exaction. Furthermore, because all results shown for Fig. 5 have $\hat{I} = 15$, the linear results for SOC versus time are all the same in Fig. 5. However, once potentiostatic extraction takes over, the result for each case diverges. Because the lithium concentration is more uniform when $\hat{\Omega} = 1500$ and $\varepsilon_{\mathrm{Li}}^{\max} = 1$, most of the lithium is extracted in this case during the galvanostatic stage, and less than 10% remains to be removed potentiostatically. Because potentiostatic extraction is always slower than galvanostatic extraction, the case of $\hat{\Omega} = 1500$ and $\varepsilon_{\mathrm{Li}}^{\max} = 1$ is the one with the most rapid removal of lithium from the storage particle over all the cases that we have considered. Reduction of $\hat{\Omega}$ or $\varepsilon_{\mathrm{Li}}^{\max}$ causes an earlier transition to potentiostatic extraction and thus to an overall slower removal of the lithium from the particle. This effect is caused by the reduction in the importance of lithium transport driven by the hydrostatic stress gradient, so that the lithium concentration gradient must be higher to maintain the surface flux of lithium at the particle surface. As a consequence, the lithium concentration at the particle surface goes to zero faster, ending galvanostatic extraction sooner. In line with the fact that $\hat{\Omega}$ controls the importance of the hydrostatic stress gradient in lithium transport, the low value used for Fig. 5(*g*) means that there is little difference among all the cases having different values of $\varepsilon_{\mathrm{Li}}^{\max}$. That is, even though a high value of $\varepsilon_{\mathrm{Li}}^{\max}$ causes high stress gradients, it has little influence on the overall rate of extraction because lithium transport is little affected by the hydrostatic stress gradient. Furthermore, the case with $\varepsilon_{\mathrm{Li}}^{\max} = 0.0$ is overall the slowest situation as far as removing 90% of the lithium is concerned. This fact is in line with the observation that the hydrostatic stress gradient driven lithium transport always speeds up extraction, so that diminishing it by making $\hat{\Omega}$ or $\varepsilon_{\mathrm{Li}}^{\max}$ low slows down the potentiostatic stage of lithium extraction as well as causing an earlier transition to it.

Figures 5(*d*) and 5(*h*) are for the special case $\hat{\Omega} = 0$. The strain here is the highest, at just over 40%. The diagram of the average SOC reveals that changing the value of $\varepsilon_{\mathrm{Li}}^{\max}$ does not affect the concentration profile, and all are identical. As noted earlier, the case of $\hat{\Omega} = 0$ implies zero contribution of the stress term to the lithium flux within the particle. The concentration profile, and therefore the SOC, is affected only by $\hat{I}$, which has the same value for all these cases.

The stresses are not plotted for the case $\varepsilon_{\mathrm{Li}}^{\max} = 0$ in Fig. 5 since they would all be zero. The SOC is plotted for $\varepsilon_{\mathrm{Li}}^{\max} = 0$ in each case. The plot for $\hat{\Omega} = 0$, $\varepsilon_{\mathrm{Li}}^{\max} = 0$ represents the baseline case; i.e., Fickian diffusion with no stresses present. This gives the lithium concentration profile that would be obtained if the stresses were not taken into account at all. As can be seen in Fig. 5, the deviation of the SOC for cases where the stress gradient has been allowed for in the lithium transport simulation, relative to the baseline, can be significant depending on the value of $\varepsilon_{\mathrm{Li}}^{\max}$ and $\hat{\Omega}$. We conclude that it is important to take the stress into account in order to predict the concentration of lithium within the particles accurately. For example, when $\hat{\Omega} = 150$ and $\varepsilon_{\mathrm{Li}}^{\max} = 0.1$ (approximately the values for lithium manganate), there is a notable difference between the SOC during potentiostatic extraction when stress driven diffusion of lithium is taken into account and when it is not.

In Fig. 6 we have plotted results for different values of $\hat{\Omega}$ together on the same graphs to enable us to encompass more values. The results are similar to, in some cases the duplicate of, those given in Fig. 5, and the same comments may be made regarding them. To avoid lengthy duplication of such comments, we abjure any description or commentary on Fig. 6, except to note that these figures allow ready comparison of results that allow for stress gradient driven lithium transport and those that do not. We observe that these differences can be considerable in terms of both the maximum principal stress and the SOC. This insight indicates, once more, that omission of stress gradient driven lithium transport is usually a mistake, leading to overestimation of the peak maximum principal stress and the SOC during extraction.

In Fig. 7 histories of the maximum principal stress for a charging rate of $\hat{I} = 1.0$ are plotted for two different values each of $\hat{\Omega}$ and $\varepsilon_{\mathrm{Li}}^{\max}$. The maximum stress reduces by an order of magnitude as compared to Fig. 5 where $\hat{I} = 15$. The lower external flux leads to a lower lithium concentration gradient within the particle, reducing the stress gradient and the stress magnitude for the reasons outlined earlier. The stress histories in Fig. 7(*a*) are similar to those in Fig. 5(*a*), but those in Figs. 7(*b*)–7(*d*) differ somewhat from their counterparts in Fig. 5. In Fig. 7, large values of $\hat{\Omega}$ and $\varepsilon_{\mathrm{Li}}^{\max}$ lead to a significant contribution from stress gradient driven lithium flux, and there is a dip in the stress profile similar to what is observed in Fig. 5(*a*).

The effect of reducing $\hat{I}$ becomes clear on inspection of the stress histories in Figs. 7(*b*)–7(*d*). There is a notable difference between the histories for $\hat{I} = 15$ observed in Figs. 5 and 6 and those for the lower current density shown in Fig. 7. Instead of a monotonic increase until the start of potentiostatic charging commonly seen at high current densities, the maximum stress either plateaus or dips, depending on the value of $\hat{\Omega}$ and $\varepsilon_{\mathrm{Li}}^{\max}$. At the lower rate of extraction, the diffusion of lithium within the particle can keep pace with the extraction of lithium from its surface, and the formation of large concentration gradients of lithium is prevented. The consequence is twofold. First, the combination of

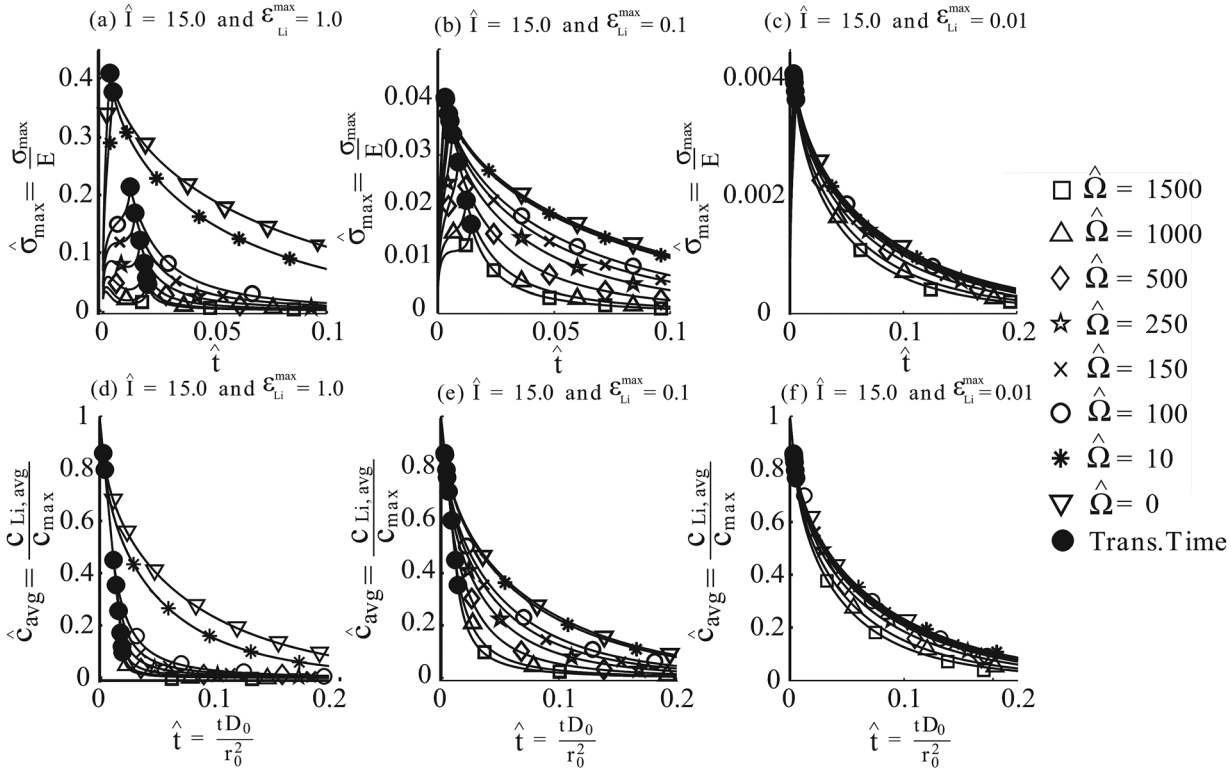

Fig. 6 Histories of maximum principal stress (*a*)–(*c*) and average lithium concentration (SOC) (*d*)–(*f*) in a storage particle during galvanostatic extraction followed by potentiostatic extraction. The normalized extraction rate is $\hat{I} = 15$ and results are shown for three values of the normalized lithiation strain ε_{Li}^{max}. Within each plot results for different values of the normalized lithium partial molar volume $\hat{\Omega}$ are provided. (*a*) Maximum principal stress for $\varepsilon_{Li}^{max} = 1.0$; (*b*) maximum principal stress for $\varepsilon_{Li}^{max} = 0.1$; (*c*) maximum principal stress for $\varepsilon_{Li}^{max} = 0.01$; (*d*) SOC for $\varepsilon_{Li}^{max} = 1.0$; (*e*) SOC for $\varepsilon_{Li}^{max} = 0.1$; and (*f*) SOC for $\varepsilon_{Li}^{max} = 0.01$.

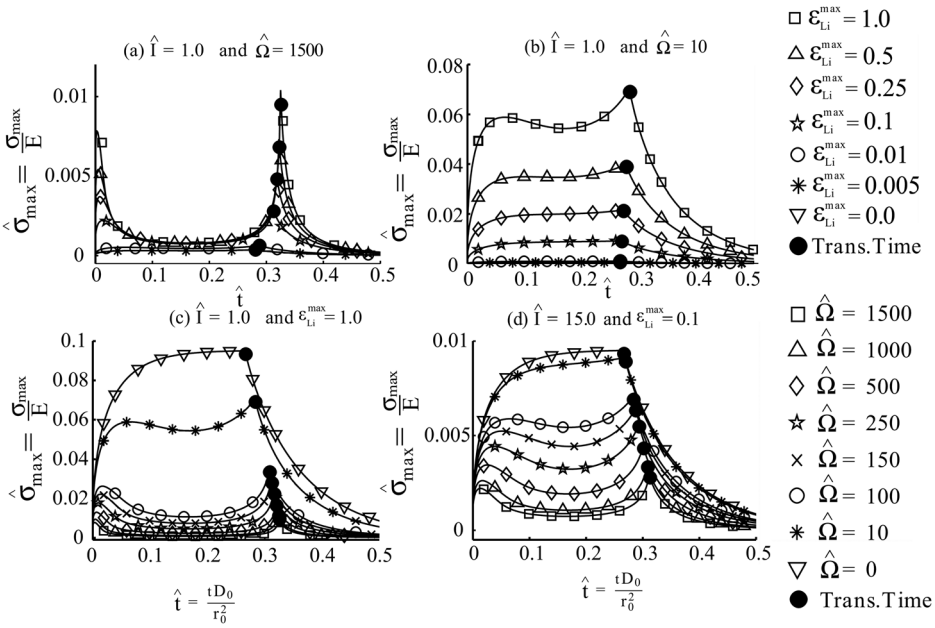

Fig. 7 Histories of maximum principal stress in a storage particle during galvanostatic extraction followed by potentiostatic extraction. The normalized extraction rate is $\hat{I} = 1.0$ and results are shown for two values of the normalized lithium partial molar volume $\hat{\Omega}$ and two values of the normalized lithiation strain ε_{Li}^{max}. In the plot for a given value of $\hat{\Omega}$ results are shown for various values of ε_{Li}^{max}, and vice versa. (*a*) Maximum principal stress for $\hat{\Omega} = 1500$; (*b*) maximum principal stress for $\hat{\Omega} = 150$; (*c*) maximum principal stress for $\varepsilon_{Li}^{max} = 1.0$; and (*d*) maximum principal stress for $\varepsilon_{Li}^{max} = 0.1$.

$\hat{\Omega}$ and $\varepsilon_{\mathrm{Li}}^{\max}$ required in order for the stress gradient to cause a significant contribution to the lithium flux will not be as high as for higher charging rates. Thus even at relatively low values of $\hat{\Omega}$ and $\varepsilon_{\mathrm{Li}}^{\max}$ a dip can be seen in the maximum stress as times passes, characteristic of cases where stress gradient driven lithium transport is playing a significant role in the diffusion process.

Second, when both values of $\hat{\Omega}$ and $\varepsilon_{\mathrm{Li}}^{\max}$ are low, the stress history will plateau. The clearest example of this is the stress profile in Fig. 7(*d*) for the case $\hat{\Omega} = 0$. In this case the stress gradient makes no contribution to the overall lithium flux. As a consequence, there is a monotonic rise in the maximum principal stress characteristic of cases where the stress gradient driven lithium flux is playing a minor role. However, since extraction of lithium is occurring at a relatively low rate, it is more likely that its diffusion in the particle matches the surface extraction rate before the transition to potentiostatic extraction occurs. This leads to the formation of a steady state lithium concentration profile. As a result, the magnitude of the stress will also stabilize, causing it to plateau until galvanostatic extraction ends.

Closure

We have attempted to give some insights into the performance and failure of lithium ion batteries through the means of a linearized one-dimensional model for the cell as whole, and through simulations of lithium transport and lithiation stress in a single spherical particle. In our approach we have tried to be as general as possible as far as combinations of performance indices and material parameters are concerned, though we have confined ourselves to idealized thermodynamics. We hope that our paper will help to advance battery design and utilization so that cells may be exploited more effectively to allow faster charging and greater exploitation of their capacity.

Dedication

We are pleased to dedicate this paper to Professor James R. Rice to mark his 70th birthday. Jim has been an inspiring and generous mentor to many, including one of the authors (RMM). As the first author of this paper is a student of RMM, Jim has directly or indirectly guided us both on our paths into research and applied mechanics. Such paths, lit by the brightness of his teaching, research, and friendship have been inspiring to follow. Jim's unforgettable kindness, creativity, and awesome intellect are recognized by all who know him, all who read his papers, and all who hear him lecture. Having been guided by Jim, RMM feels fortunate. With this paper on lithium ion batteries, the authors wish to honor Jim. Though lithium ion batteries is a subject that Jim has not worked on, the topic involved—applied mechanics coupled to thermodynamics and chemistry—is one where Jim did pioneering work, and so the authors owe much to Jim regarding the genesis of this work.

Acknowledgment

The research in this paper is supported by a contract with the Robert Bosch Corporation and a grant from the University of California Discovery Program. We thank Esther Bohn and Thomas Eckl from Robert Bosch GmbH, Stuttgart, Germany for stimulating discussions and valuable comments.

References

[1] Besenhard, J. O., 1998, *Handbook of Battery Materials*, Wiley-VCH, New York.
[2] Nazri, G.-A., and Pistoia, G., Eds., *Lithium Batteries: Science and Technology*, Kluwer, Dordrecht, Netherlands.
[3] Christensen, J., and Newman, J., 2006, "A Mathematical Model of Stress Generation and Fracture in Lithium Manganese Oxide," J. Electrochem. Soc., **153**, pp. A1019–A1030.
[4] Vetter, J., Novak, P., Wagner, M. R., Veit, C., Moeller, K.-C., Besenhard, J. O., Winter, M., Wohlfahrt-Mehrens, M., Vogler, C., and Hammouche, A., 2005, "Ageing Mechanisms in Lithium-Ion Batteries," J. Power Sources, **147**, pp. 269–281.
[5] Moon, H. S., Lee, W., Reucroft, P. J., and Park, J.-W., 2003, "Effect of Film Stress on Electrochemical Properties of Lithium Manganese Oxide Thin Films," J. Power Sources, **119–121**, pp. 710–712.
[6] Wang, D., Wu, X., Wang, Z., and Chen, L., 2005, "Cracking Causing Cyclic Instability of $LiFePO_4$ Cathode Material," J. Power Sources, **140**, pp. 125–128.
[7] Christensen, J., and Newman, J., 2006, "Stress Generation and Fracture in Lithium Insertion Materials," J. Solid State Electrochem., **10**, pp. 293–319.
[8] Taberna, L., Mitra, S., Poizot, P., Simon, P., and Tarascon, J.-M., 2006, "High Rate Capabilities of Fe_3O_4-Based Cu Nano-architectured Electrodes for Lithium-Ion Battery Applications," Nat. Mater., **5**, pp. 567–573.
[9] Tarascon, J.-M., and Armand, M., 2001, "Issues and Challenges Facing Rechargeable Batteries," Nature, **414**, pp. 359–367.
[10] Sethuraman, V. A., Srinivasan, V., Bower, A. F., and Guduru, P. R., 2010, "In Situ Measurements of Stress-Potential Coupling in Lithiated Silicon," J. Electrochem. Soc., **157**, pp. A1253–A1261.
[11] Broussely, M., 2002, "Ageing Mechanisms and Calendar-Life Predictions," in *Advances in Lithium-Ion Batteries*, W. van Schalkwijk and B. Scrosati, Eds., Kluwer Academic/Plenum, Dordrecht, Netherlands,, pp. 393–432.
[12] Bloom, I., Cole, B. W., Sohn, J. J., Jones, S. A., Polzin, E. G., Battaglia, V. S., Henriksen, G. L., Motloch, C. G., Richardson, R., Unkelhaeuser, T., Ingersoll, D., and Case, H. L., 2001, "An Accelerated Calendar and Cycle Life Study of Li-Ion Cells," J. Power Sources, **101**, pp. 238–247.
[13] Wright, R. B., Motloch, C. G., Belt, J. R., Christophersen, J. P., Ho, C. D., Richardson, R. A., Bloom, I., Jones, S. A., Battaglia, V. S., Henriksen, G. L., Unkelhaeuser, T., Ingersoll, D., Case, H. L., Rogers, S. A., and Sutula, R. A., 2002, "Calendar- and Cycle-Life Studies of Advanced Technology Development Program Generation I Lithium-Ion Batteries," J. Power Sources, **110**, pp. 445–470.
[14] Abraham, D. P., Liu, J., Chen, C. H., Hyung, Y. E., Stoll, M., Elsen, N., MacLaren, S., Twesten, R., Haasch, R., Sammann, E., Petrov, I., Amine, K., and Henriksen, G., 2003, "Diagnosis of Power Fade Mechanisms in High-Power Lithium-Ion Cells," J. Power Sources, **119–121**, pp. 511–516.
[15] Bloom, I., Jones, S. A., Battaglia, V. S., Henriksen, G. L., Christophersen, J. P., Wright, R. B., Ho, C. D., Belt, J. R., and Motloch, C. G., 2003, "Effect of Cathode Composition on Capacity Fade, Impedance Rise and Power Fade in High-Power, Lithium-Ion Cells," J. Power Sources, **124**, pp. 538–550.
[16] Bloom, I., Potter, B. G., Johnson, C. S., Gering, K. L., and Christophersen, J. P., 2006, "Effect of Cathode Composition on Impedance Rise in High-Power Lithium-Ion Cells: Long-Term Aging Results," J. Power Sources, **155**, pp. 415–419.
[17] Peabody, C., and Arnold, C. B., 2011, "The Role of Mechanically Induced Separator Creep in Lithium-Ion Battery Capacity Fade," J. Power Sources, **196**, pp. 8147–8153.
[18] Doyle, M., Fuller, T. F., and Newman, J., 1993, "Modeling of Galvanostatic Charge and Discharge of the Lithium/Polymer/Insertion Cell," J. Electrochem. Soc., **140**, pp. 1526–1533.
[19] Thomas, K. E., Darling, R. M., and Newman, J., 2002, "Mathematical Modeling of Lithium Batteries," in *Advances in Lithium-Ion Batteries*, W. van Schalkwijk and B. Scrosati, eds., Kluwer Academic/Plenum, Dordrecht, Netherlands, pp. 345–392.
[20] Darling, R., and Newman, J., 1997, "On the Short-Time Behavior of Porous Intercalation Electrodes," J. Electrochem. Soc., **144**, pp. 3057–3063.
[21] Ning, G., and Popov, B. N., 2004, "Cycle Life Modeling of Lithium-Ion Batteries," J. Electrochem. Soc., **151**, pp. A1584–A1591.
[22] Devan, S., Subramanian, V. R., and White, R. E., 2005, "Transient Analysis of a Porous Electrode," J. Electrochem. Soc., **152**, pp. A947–A955.
[23] Ning, G., White, R. E., and Popov, B. N., 2006, "A Generalized Cycle Life Model of Rechargeable Li-Ion Batteries," Electrochim. Acta, **51**, pp. 2012–2022.
[24] Stephenson, D. E., Hartman, E. M., Harb, J. N., and Wheeler, D. R., 2007, "Modeling of Particle-Particle Interactions in Porous Cathodes for Lithium-Ion Batteries," J. Electrochem. Soc., **154**, pp. A1146–A1155.
[25] Renganathan, S., Sikha, G., Santhanagopalan, S., and White, R. E., 2010, "Theoretical Analysis of Stresses in a Lithium Ion Cell," J. Electrochem. Soc., **157**, pp. A155–A163.
[26] Christensen, J., 2010, "Modeling Diffusion Induced Stress in Li-Ion Cells With Porous Electrodes," J. Electrochem. Soc., **157**, pp. A366–A380.
[27] Garcia, R. E., Chiang, Y.-M., Carter, W. C., Limthongkul, P., and Bishop, C. M., 2005, "Microstructural Modeling and Design of Rechargeable Lithium-Ion Batteries," J. Electrochem. Soc., **152**, pp. A255–A263.
[28] Garcia, R. E., and Chiang, Y.-M., 2007, "Spatially Resolved Modeling of Microstructurally Complex Battery Architectures," J. Electrochem. Soc., **154**, pp. A856–A864.
[29] Yi, Y.-B., Wang, C.-W., and Sastry, A. M., 2006, "Compression of Packed Particulate Systems: Simulations and Experiments in Graphitic Li-Ion Anodes," ASME J. Eng. Mater. Technol., **128**, pp. 73–80.
[30] Zhang, X., Shyy, W., and Sastry, A. M., 2007, "Numerical Simulation of Intercalation-Induced Stress in Li-Ion Battery Electrode Particles," J. Electrochem. Soc., **154**, pp. A910–A916.
[31] Park, J., Lu, W., and Sastry, A. M., 2011, "Numerical Simulation of Stress Evolution in Lithium Manganese Dioxide Particles Due to Coupled Phase Transition and Intercalation," J. Electrochem. Soc., **158**, pp. A201–A206.
[32] Ploehn, H. J., Ramadass, P., and White, R. E., 2004, "Solvent Diffusion Model for Aging of Lithium-Ion Battery Cells," J. Electrochem. Soc., **151**, pp. A456–A462.

[33] Chen, Y., and Evans, J. W., 1994, "Three-Dimensional Thermal Modeling of Lithium-Polymer Batteries Under Galvanostatic Discharge and Dynamic Power Profile," J. Electrochem. Soc., **141**, pp. 2947–2955.
[34] Newman, J., and Tiedemann, W., 1995, "Temperature Rise in Battery Module With Constant Heat Generation," J. Electrochem. Soc., **142**, pp. 1054–1057.
[35] Chen, Y., and Evans, J. W., 1996, "Thermal Analysis of Lithium-Ion Batteries," J. Electrochem. Soc., **143**, pp. 2708–2712.
[36] Pals, C. R., and Newman, J., 1995, "Thermal Modeling of Lithium/Polymer Battery, I Discharge Behavior of a Single Cell," J. Electrochem. Soc., **142**, pp. 3274–3281.
[37] Song, L., and Evans, J. W., 2000, "Electrochemical-Thermal Modeling of Lithium Polymer Batteries," J. Electrochem. Soc., **147**, pp. 2086–2095.
[38] Golmon, S., Maute, K., and Dunn, M. L., 2009, "Numerical Modeling of Electrochemical-Mechanical Interactions in Lithium Polymer Batteries," Comput. Struct., **87**, pp. 1567–1579.
[39] Bohn, E., Eckl, T., Kamlah, M., and McMeeking, R. M., 2011, "A Model for Lithium Diffusion and Stress Generation in a Storage Particle of an Intercalation Electrode," submitted.
[40] Verbrugge, M. W., and Koch, B. J., 1996, "Modeling Lithium Intercalation of Single-Fiber Carbon Microelectrodes," J. Electrochem. Soc., **143**, pp. 600–608.
[41] Aifantis, K. E., and Dempsey, J. P., 2005, "Stable Crack Growth in Nanostructured Li-Batteries," J. Power Sources, **143**, pp. 203–211.
[42] Cheng, Y.-T., and Verbrugge, M. W., 2010, "Application of Hasselman's Crack Propagation Model to Insertion Electrodes," Electrochem. Solid State Lett., **13**, pp. A128–A131.
[43] Cheng, Y.-T., and Verbrugge, M. W., 2010, "Diffusion-Induced Stress, Interfacial Charge Transfer, and Criteria for Avoiding Crack Initiation of Electrode Particles," J. Electrochem. Soc., **157**, pp. A508–A516.
[44] Zhao, K., Pharr, M., Vlassak, J. J., and Suo, Z., 2010, "Fracture of Electrodes in Lithium-Ion Batteries Caused by Fast Charging," J. Appl. Phys., **108**, p. 073517.
[45] Yang, F., 2010, "Insertion-Induced Breakage Materials," J. Appl. Phys., **108**, p. 073536.
[46] Woodford, W. H., Chiang, Y.-M., and Carter, W. C., 2010, "Electrochemical Shock' of Intercalation Electrodes—A Fracture Mechanics Analysis," J. Electrochem. Soc., **157**, pp. A1052–A1059.
[47] Bhandakkar, T. K., and Gao, H., 2010, "Cohesive Modeling of Crack Nucleation Under Diffusion Induced Stresses in a Thin Strip: Implications on the Critical Size for Flaw Tolerant Battery Electrodes," Int. J. Solids Struct., **47**, pp. 1424–1434.
[48] Bhandakkar, T. K., and Gao, H., 2011, "Cohesive Modeling of Crack Nucleation in a Cylindrical Electrode Under Axisymmetric Diffusion Induced Stresses," Int. J. Solids Struct., **48**, pp. 2304–2309.
[49] Bower, A. F., Guduru, P. R., and Sethuraman, V. A., 2011, "A Finite Strain Model of Stress, Diffusion, Plastic Flow, and Electrochemical Reactions in a Lithium-Ion Half Cell," J. Mech. Phys. Solids, **59**, pp. 804–828.
[50] Zhao, K., Pharr, M., Vlassak, J. J., and Suo, Z., 2011, "Inelastic Hosts As Electrodes for High-Capacity Lithium-Ion Batteries," J. Appl. Phys., **109**, p. 016110.
[51] Botte, G. G., and White, R. E., 2001, "Modeling Lithium Intercalation in a Porous Carbon Electrode," J. Electrochem. Soc., **148**, pp. A54–A66.
[52] Subramanian, V. R., Boovaragavan, V., Ramadesigan, V. Chen, K., and Braatz, R. D., 2009, "Model Reformulation and Design of Lithium-Ion Batteries," *Design for Energy and the Environment*, A. A. Linniger and M. M. El-Hawagi, eds., Taylor and Francis, London, pp. 987–1005.
[53] Renganathan, S., and White, R. E., 2011, "Semianalytical Method of Solution for Solid Phase Diffusion in Lithium Ion Battery Electrodes: Variable Diffusion Coefficient," J. Power Sources, **196**, pp. 442–448.
[54] Ramadesigan, V., Boovaragavan, V., Pirkle, J. C., Jr., and Subramanian, V. R., 2010, "Efficient Reformulation of Solid-Phase Diffusion in Physics-Based Lithium-Ion Battery Models," J. Electrochem. Soc., **157**, pp. A854–A860.
[55] Forman, J. C., Bashash, S., Stein, J. L., and Fathy, H. K., 2011, "Reduction of the Electrochemistry-Based Li-Ion Battery Model Via Quasi-Linearization and Padé Approximation," J. Electrochem. Soc., **158**, pp. A93–A101.
[56] Gallagher, K. G., Nelson, P. A., and Dees, D. W., 2011, "Simplified Calculation of the Area Specific Impedance for Battery Design," J. Power Sources, **196**, pp. 2289–2297.
[57] Newman, J., and Thomas-Alyea, K. E., 2004, *Electrochemical Systems*, 3rd ed., John Wiley, Hoboken, NJ.
[58] Doyle, M., Newman, J., Gozdz, A., Schmutz, C., and Tarascon, J. M., 1996, "Comparison of Modeling Predictions With Experimental Data From Plastic Lithium Ion Cells," J. Electrochem. Soc., **143**, pp. 1890–1903.
[59] Darling, J., and Newman, J., 1999, "Dynamic Monte Carlo Simulations of Diffusion in $Li_yMn_2O_4$," J. Electrochem. Soc., **146**, pp. 3765–3772.
[60] Cheng, Y.-T., and Verbrugge, M., 2009, "Evolution of Stress Within a Spherical Insertion Electrode Particle Under Potentiostatic and Galvanostatic Operation," J. Power Sources, **190**, pp. 453–460.
[61] Timoshenko, S. P., and Goodier, J. N., 1951, *Theory of Elasticity*, 2nd ed., McGraw-Hill, New York.
[62] Yang, F., 2005, "Interaction Between Diffusion and Chemical Stresses," Mater. Sci. Eng., **A-409**, pp. 153–159.